SERBIAN ACADEMY OF SCIENCES AND ARTS
СРПСКА АКАДЕМИЈА НАУКА И УМЕТНОСТИ

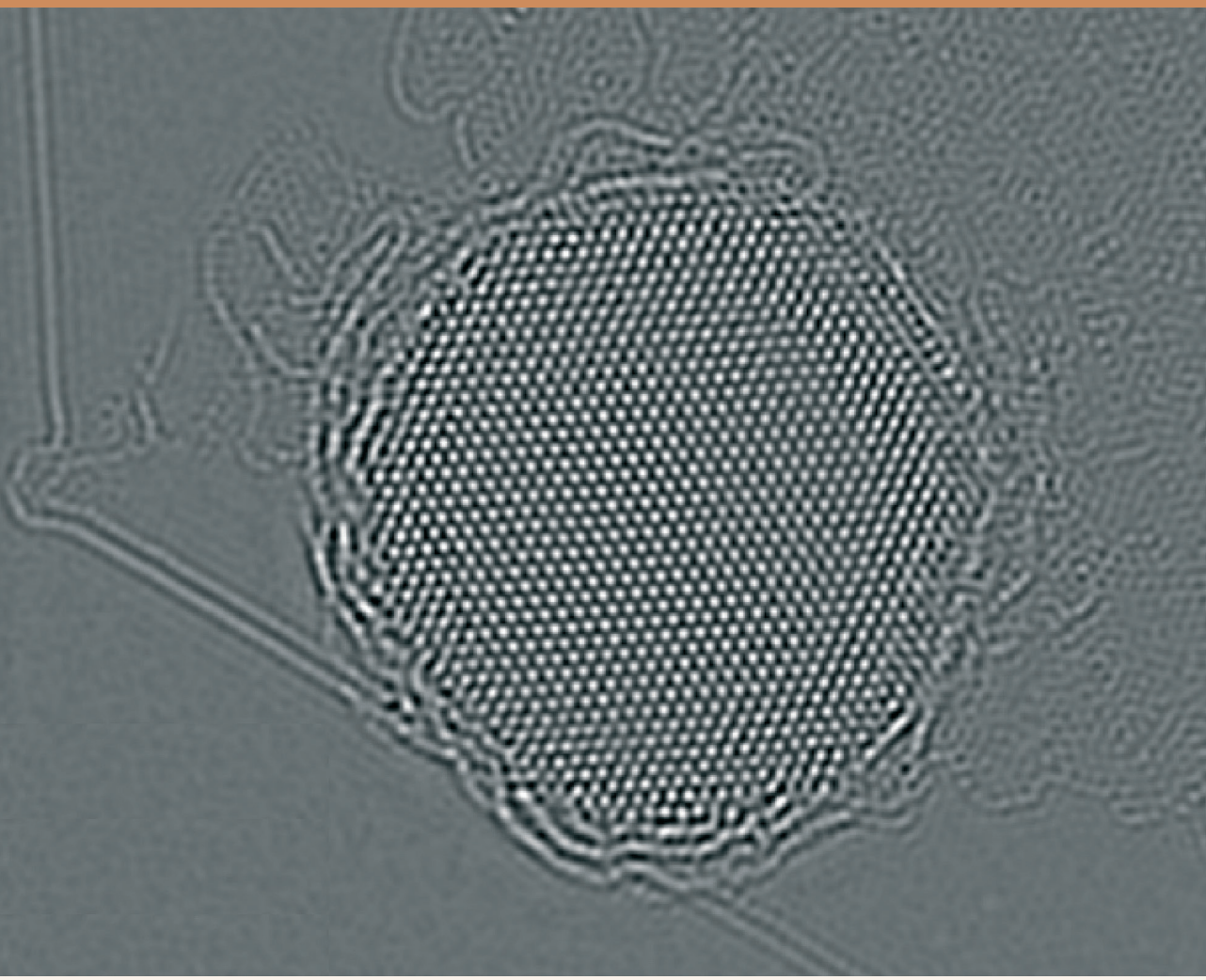

FASCINATING WORLD OF NANOSCIENCES AND NANOTECHNOLOGIES
ФАСЦИНАНТНИ СВЕТ НАНОНАУКА И НАНОТЕХНОЛОГИЈА

FASCINATING WORLD OF NANOSCIENCES AND NANOTECHNOLOGIES

ФАСЦИНАНТНИ СВЕТ НАНОНАУКА И НАНОТЕХНОЛОГИЈА

СРПСКА АКАДЕМИЈА НАУКА И УМЕТНОСТИ

ЦИКЛУС ПРЕДАВАЊА

Књига 6

ФАСЦИНАНТНИ СВЕТ НАНОНАУКА И НАНОТЕХНОЛОГИЈА

Примљено на I скупу Одељења техничких наука,
одржаном 22. јануара 2020. године

Уредници
ВЕЛИМИР Р. РАДМИЛОВИЋ
Српска академија наука и уметности
и
ЏЕФ Т. М. ДЕХОСОН
Холандска краљевска академија наука и уметности

БЕОГРАД 2020

SERBIAN ACADEMY OF SCIENCES AND ARTS

LECTURE SERIES

Book 6

FASCINATING WORLD OF NANOSCIENCE AND NANOTECHNOLOGY

Accepted at the 1st meeting of the Department of Technical Sciences
held on January 22, 2020

Editors
VELIMIR R. RADMILOVIĆ
Serbian Academy of Sciences and Arts
and
JEFF TH. M. DEHOSSON
Royal Netherlands Academy of Arts and Sciences

BELGRADE 2020

Published by
Serbian Academy of Sciences and Arts
Belgrade, 35 Kneza Mihaila St.

Reviewers
Prof. Dr. Dragan Uskoković
Prof. Dr. Djordje Janaćković

Copy editing for English
Jelena Mitrić and Vuk V. Radmilović

Proofreader
Nevena Đurđević

Translation of Summaries
Vuk V. Radmilović

Technical editor
Nikola Stevanović

Print run
400 copies

Printed by
Planeta print

ISBN 978-86-7025-859-4

Издаје
Српска академија наука и уметности
Београд, Кнеза Михаила 35

Рецензенти
Проф. др Драган Ускоковић
Проф. др Ђорђе Јанаћковић

Лектура
Јелена Митрић и Вук В. Радмиловић

Коректура
Невена Ђурђевић

Превод резимеа
Вук В. Радмиловић

Технички уредник
Никола Стевановић

Тираж
400 примерака

Штампа
Планета принт

ISBN 978-86-7025-859-4

CONTENTS

FASCINATING WORLD OF NANOSCIENCE AND NANOTECHNOLOGY

Researchers whose work has led to significant discoveries, looking much further, beyond the immediate resolution of technical problems, are asking themselves important questions such as: why individual phenomena occur, how they develop, and why they work. In order to enhance our knowledge about the world around us, and to see pictures of worlds that elude the human eye, through history many experimental and theoretical methods have been developed and are still being improved, including the development of telescopes and microscopes, which enable us to see "very large" and "very small" things.

Researchers involved in the "big things" (the universe, galaxies, stars and planets) have found that a galaxy of an average size of about 100.000 light-years has, on average, around one quadrillion (10^{15}) stars. Researchers involved in the "little things" (nanostructures, molecules, clusters of atoms, individual atoms, atomic defects, etc.) have discovered that 1 cm3 of aluminum alloys also contains approximately one quadrillion (10^{15}) nanoparticles that strengthen these alloys in order to be utilized as a structural material for aircrafts, without which modern transport is unimaginable. How do we count the number of stars in a galaxy or the number of nanoparticles in an aluminum alloy? Relatively easy, because we can see the nanoparticles in aluminum alloys using electron microscopes, and stars in a galaxy using telescopes. Scientific discoveries form the basis for scientific and technological progress, and one such example are the discoveries in the fields of nanosciences and nanotechnologies.

Why is this monograph dedicated to nanosciences and nanotechnologies?

To answer this question, we must first answer the question: what are nanoscience and nanotechnology? In the inevitable *Wikipedia*, *Encyclopedia Britannica* (and any other encyclopedia), dictionaries as well as internet sources, the terms "nanoscience" and "nanotechnology" are related to the study, understanding, controlled manipulation of structures and phenomena, and the application of extremely small things, which have at least one dimension less than 100 nm. Modern aspects of nanosciences and nanotechnologies are quite new and have been developing intensively in the last twenty to thirty years, but the nanoscale substances have been used for centuries, if not millennia. Particulate pigments, for example, have been used in ancient China, Egypt, etc., several thousands of years ago. Artists have decorated windows in medieval churches using silver and gold nanoparticles of various sizes and composition, without understanding the origin of the various colors. Nanoparticles that strengthen alloys of iron, aluminum and other metals, have been used for over a hundred years, although they have not been branded with a prefix "nano", but rather called "precipitates". Scientific disci-

plines, involved in significant research activities related to nanoscience and nanotechnology, are: physical metallurgy, materials science and materials engineering, chemistry, physics, biology, electrical engineering, and so on.

Where does the prefix "nano" come from? "Nano" comes from the Greek words *νᾶνος*, which means a dwarf, indicating a dimension of one nanometer (1 nm), which represents one-billionth (10^{-9}) of a meter; Similarly, "nanosecond" (ns) denotes a billionth of a second, and so on. This sounds a bit abstract to many, but to put things into context with which we are familiar, we can mention that the diameter of a human hair, for example, is on average about 100.000 nm (10^5 nm = 100 microns = 0.1 mm), which is roughly the bottom threshold of human eye detection; Thickness of newsprint on average is also about 100.000 nm = 100 μm = 0.1 mm; Person of 2 m height is 2.000.000.000 (2×10^9) nm high. For comparison, if we assume that the diameter of a children's glass marble was 1 nm, then the diameter of the Earth would be 1 m.

When we talk about the structures of inorganic, organic and bio-nanosystems, their dimensions are as follows: Diameter of carbon atom is in the order of 0.1 nm, or one-tenth of a billionth of a meter; Single-wall carbon nanotubes have a diameter of around 2 nm, or 2 billionth of a meter; The width of the deoxyribonucleic acid (DNA) chain is also about 2 nm, or 2 billionths of a meter; Proteins, which can vary in size, depending on how many amino acids they are composed of, are in the range mainly between 2 and 10 nm, or between 2 and 10 billionths of a meter (assuming their spherical shape); Diameter of individual molecules of hemoglobin is about 5 nm, or 5 billionths of a meter.

Indeed, these are small sizes, but why should they be important, or why does size matter? When analyzing physical systems on the nanoscale, their fundamental properties change drastically. Consider the example, melting point of gold: transition temperature of solid to liquid for gold nanoparticles ~4 nm in size, is about 400°C, while the melting temperature of bulk (macroscopic) gold is 1063°C. The same can be said for other properties: mechanical properties, electric conductivity, magnetism, chemical reactivity, etc., also may be drastically changed, which means that nanosystems deviate from the laws of classical physics that describe the motion of the planets, the direction of movement of a rockets which carry satellites to explore space, etc. The base of this fascinating behavior of nanostructures are bonds between the atoms. As structures become smaller, more atoms are present on the surface, hence the ratio of the surface area to volume for these structures increases dramatically. It results in a dramatic change of physicochemical properties of nanostructures from the bulk, as well as possible appearance of quantum effects: nanoscale structures become stronger, less brittle, demonstrate enhanced optical and catalytic properties, and generally, are very different compared to the usual, macroscopic system dimensions to which we are accustomed to in everyday practice.

This monograph comprises a number of contributions which illustrate the sparkling and fascinating world of nanoscience and nanotechnology.

Nanoporous organometallic materials, that can mimic the properties of muscles upon outside stimuli, are ideal actuators, thereby offering a unique combination of low operating voltages, relatively large strain amplitudes, high stiffness and strength. These phenomena are discussed in the manuscript of J. Th. M. DeHosson and E. Detsi.

Drugs in nanodimension range will become much more efficient with reduced adverse effects. A typical example are drugs, carried by various types of nanoparticles which have been previously functionalized, so as to only recognize diseased cells which is a highly selective medical procedure on a molecular level. Besides drugs, functionalized nanoparticles can carry radioactive material or a magnetic structure, which in a strong magnetic field develop high temperatures, and destroy cancer cells. Some aspects of electron microscopy utilized in the study of biological nanostructures are discussed in the paper of A. E. Porter and I. G. Theodorou.

Increased production of nanomaterials raises concern about their safety, not only for humans but also for animals and the environment as well. Their toxicity depends on nanoparticle size, shape, surface area, surface chemistry, concentration, dispersion, aggregation, route of administration and many other factors. The review by M. Čolić and S. Tomić summarizes the main aspects of nano-toxicity in vitro and in vivo, points out relevant tests of demonstrating toxicity and explains the significance of reactive oxygen species, as the main mechanism of nanoparticle cytotoxicity and genotoxicity through the complex interplay between nanoparticles and cellular or genomic components.

Carbon nanomaterials are a large group of advanced materials that are in focus of extensive research, due to their interesting properties and versatile applicability, especially carbon nanostructures doped by covalently bonded heteroatoms (N, B, P, etc.) which leads to improved properties. This topic is discussed in the manuscript by G. Ćirić-Marjanović.

Combinations of optical, magnetic and photocatalytic properties of nanomaterials, especially those with large energy gaps, are of great interest for nanoscience and nanotechnology. One of such systems are TiO2 nanostructures with different crystal lattices and shapes (spheres, nanotubes, nanorods), either pure or hybrid, in the form of nanocomposites with matrices based on conducting polymers, which is presented in the work of Z. Šaponjić and coauthors.

Design and manufacturing of multifunctional nanomaterials is one of the most important trends in materials nanoscience, where combining nanomaterials of various characteristics, such as ferroelectrics, ferromagnetics and ferroelastics can lead to achieving adequate multifunctionality, a good example of which are multiferroic nanomaterials, presented in the work of V. Srdić and coauthors.

Materials containing crystal grains of nanodimensions can demonstrate dramatically improved properties. Theoretically as well as experimentally, it has been shown that metallic nanostructures can attain a high percentage of theoretical strength, which questions the classical definition of material strength, stated

until recently by textbooks that does not depend on size of a tested sample. Some aspects of mechanisms of formation, growth and shrinking of crystal grains are discussed in the paper of T. Radetić.

Computational methods, including first principal calculations, have been proven to be a powerful tool in allowing investigations of systems of various complexities, spatial and temporal scales. This allows for screening of a large number of systems, which is not experimentally feasible, and also the understanding of general trends which is of great importance for both theoreticians and experimentalists. The use of this concept in applications of metallic and oxide nanoparticles is described in manuscript of I. A. Pašti and coauthors.

Being aware of the importance of nanosciences and nanotechnologies and their global impact on humanity, in the autumn of 2017, Serbian Academy of Sciences and Arts launched a series of lectures dedicated to these topics from which this monograph arose. We hope that this monograph will be of interest to the reader and can serve as a motivation for creating opportunity for research to those who want to find out more about these fascinating fields of sciences and technologies.

Velimir R. Radmilović
Serbian Academy of Sciences and Arts

Jeff Th. M. DeHosson
Royal Netherlands Academy of Arts and Sciences

ФАСЦИНАНТНИ СВЕТ НАНОНАУКА И НАНОТЕХНОЛОГИЈА

Истраживачи чији је рад довео до значајних открића гледају много даље, изван непосредног решавања техничких проблема, постављају себи важна питања, као што су: зашто се дешавају одређене појаве, како се оне развијају и на који начин функционишу? Кроз историју је развијен велики број експерименталних и теоријских метода, које се и дан-данас унапређују, како бисмо обогатили знање о свету који нас окружује и могли да видимо слике светова који измичу људском оку, укључујући ту и проналазак телескопа и микроскопа, који нам омогућавају да видимо „веома велике" и „веома мале" ствари.

Истраживачи који се баве „великим стварима" (универзумом, галаксијама, звездама и планетама) установили су да једна галаксија, око 100.000 светлосних година, у просеку садржи око једну билијарду (10^{15}) звезда. Истраживачи који се баве „малим стварима" (наноструктурама, молекулима, кластерима атома, појединачним атомима, атомским дефектима итд.) установили су да 1 cm^3 легуре алуминијума садржи око једну билијарду (10^{15}) наночестица које ојачавају ту легуру, како би могла да се користи као материјал за израду ваздухоплова, без којих је савремени транспорт незамислив. Како можемо пребројати звезде у једној галаксији или наночестице у једној легури алуминијума? Релативно лако, зато што уз помоћ електронских микроскопа можемо видети наночестице у легурама алуминијума, а звезде у галаксијама уз помоћ телескопа. Научна открића представљају основу научног и технолошког напретка, а један такав пример су открића у области нанонаука и нанотехнологија.

Зашто је ова монографија посвећена нанонаукама и нанотехнологијама?

Да бисмо одговорили на ово питање најпре морамо да установимо шта су то нанонауке и нанотехнологије? Према неизбежној Википедији, Енциклопедији Британици (или било којој другој енциклопедији), речницима, као и изворима са интернета, појмови „нанонаука" и „нанотехнологија" се односе на проучавање, разумевање, контролисано манипулисање структурама и појавама, као и на примену изузетно малих честица, чија је најмање једна димензија у опсегу до 100 nm. Иако су савремени аспекти нанонаука и нанотехнологија сасвим нови и интензивно се развијају у последњих двадесет до тридесет година, облици материје на нано скали користе се већ вековима, ако не и миленијумима. На пример, одређени пигменти коришћени су још у древној Кини и Египту, пре неколико хиљада година. Уметници су украшавали прозоре на средњовековним црквама користећи сребрне и златне наночестице различите величине и састава, при чему нису знали одакле потичу разне боје. Наночестице којима се ојачавају легуре гвожђа, алуминијума и других метала, користе се већ више од сто година,

иако у њиховом називу није садржан префикс „нано", већ се обично називају „талози". Научне дисциплине које су укључене у значајне истраживачке активности у области нанонауке и нанотехнологије су: физичка металургија, наука о материјалима и инжењерство материјала, хемија, физика, биологија, електротехника, и тако даље.

Одакле потиче префикс „нано"? Префикс „нано" потиче од грчке речи *νᾶνος*, што значи патуљак, указујући тако на димензију од једног нанометра (1 nm) која представља милијардити део метра (10^{-9} m). Слично томе, „наносекунда" (ns) означава милијардити део секунде. Ово многима може звучати помало апстрактно, међутим, ствари можемо да поставимо у контекст који је нама познат, и да поменемо, на пример, да пречник власи људске косе у просеку износи 100.000 nm (10^5 nm = 100 микрона = 0.1 mm), што отприлике представља праг онога што може да се опази голим оком. Дебљина новинског папира у просеку такође износи око 100.000 nm = 100 μm = 0.1 mm. Особа висине 2 m висока је 2.000.000.000 (2×10^9) nm. Поређења ради, ако претпоставимо да је пречник дечијег кликера 1 nm, онда би пречник планете Земље износио 1 m.

Када говоримо о структурама неорганских, органских и природних наносистема, њихове димензије су следеће: пречник атома угљеника је реда величине 0.1 nm, а то је једна десетина милијардитог дела метра; једнозидне угљеничне наноцеви имају пречник од око 2 nm, а то су два милијардита дела метра; ширина ланца дезоксирибонуклеинске киселине (ДНК) такође износи око 2 nm, а то су два милијардита дела метра; пречник протеина, чија величина често варира у зависности од тога од колико се амино киселина састоје, реда је величине 2–10 nm, или између два и десет милијардитих делова метра (под претпоставком да су сферног облика); пречник појединачних молекула хемоглобина износи око 5 nm, или 5 милијардитих делова метра.

Уистину, ово су све мале димензије, али зашто би оне уопште требало да буду важне, или зашто је величина битна? Када се анализирају физички системи на нано скали, њихова основна својства се драстично мењају. Размотримо, на пример, тачку топљења злата: температура на којој наночестице злата реда величине ~4 nm прелазе из чврстог у течно стање износи око 400°C, док је температура топљења макроскопских узорака злата 1063°C. На исти начин мењају се и неке друге особине: механичке особине, електрична проводљивост, магнетизам, хемијска реактивност итд. могу драстично да се промене, што значи да наносистеми одступају од закона класичне физике који описују кретање планета, правац кретања ракета које носе сателите за истраживање свемира итд. Ово фасцинантно понашање наноструктура потиче од веза између атома. Што су структуре мање, то је више атома присутно на површини, услед чега се однос површине и запремине ових структура драстично повећава. Као последица јавља се драматична промена физичко-хемијских својстава наноструктура у односу на структуре макроскопских димензија, као и могућа појава квантних ефеката: структуре на нано скали

постају чврше, мање крте, показују боља оптичка и каталитичка својства, и, уопштено, веома се разликују од структура уобичајених, макроскопских димензија, које сусрећемо у свакодневној пракси.

Ова монографија садржи низ радова који илуструју фасцинантан свет нанонаука и нанотехнологија.

Нанопорозни органометални материјали, који могу да опонашају особине мишића изложених спољашњим подстицајима, идеални су покретачи, који нуде јединствену комбинацију малих радних напона, релативно велике амплитуде напрезања, велику крутост и снагу. Ове појаве су описане у раду чији су аутори Ц. Т. М. ДеХосон и Е. Детси.

Лекови у области нанодимензија ће постати много ефикаснији и са смањеним штетним ефектима. Типичан пример су лекови које преносе различити типови наночестица, а које су претходно функционализоване тако да препознају само оболеле ћелије, што представља високо селективан поступак на молекуларном нивоу. Поред лекова, функционализоване наночестице могу да буду носачи радиоактивног материјала или магнетних структура, који у јаком магнетном пољу развијају високе температуре и тако уништавају ћелије рака. Одређени аспекти електронске микроскопије који се користе у проучавању биолошких наноструктура описани су у радовима чији су аутори А. Е. Портер и И. Г. Теодору.

Повећана производња наноматеријала изазива забринутост везану за њихову безбедност, не само по здравље људи, већ и за животиње и животну средину. Њихова токсичност зависи од величине наночестица, њиховог облика, величине и хемије површине, концентрације, дисперзије, склоности ка стварању агломерата, начина примене, као и многих других фактора. Рад чији су аутори М. Чолић и С. Томић даје преглед главних аспеката нанотоксичности ин витро и ин виво, указује на релевантне тестове за утврђивање токсичности, појашњава значај реактивности молекула кисеоника, као главног механизма цитотоксичности и генотоксичности наночестица кроз сложено међудејство наночестица и ћелијских или генских компоненти.

Угљенични наноматеријали представљају велику групу напредних материјала, који због својих занимљивих својстава и широке примењивости заузимају централно место у опсежним истраживањима, нарочито када су у питању угљеничне наноструктуре допиране разнородним атомима, повезаних ковалентним везама (N, B, P итд.), што доводи до побољшања њихових својстава. Ову тему обрађује рад чији је аутор Г. Ћирић-Марјановић.

Комбинације оптичких, магнетских и фотокаталитичких својстава наноматеријала, нарочито оних са великим енергијским процепом, од велике су важности за нанонауке и нанотехнологије. Један од таквих система су TiO_2 наноструктуре са различитим кристалним решеткама и облицима (наносфере, наноцеви, наноштапићи), у чистом или хибридном облику, у облику нанокомпозита са основама које су на бази проводних полимера, што је представљено у раду З. Шапоњића и сарадника.

Пројектовање и производња мултифункционалних наноматеријала представљају један од најважнијих трендова у нанонауци о материјалима, где комбиновање наноматеријала који поседују различита својства, попут фероелектричности, феромагнетизма и фероеластичности, може довести до постизања одговарајуће мултифункционалности, чији су добар пример мултифероични наноматеријали, који су представљени у раду В. Срдића и сарадника.

Материјали који садрже кристална зрна нанодимензија показују знатно побољшане особине. Теоријски и експериментално је показано да металне наноструктуре могу да достигну висок проценат теоријске чврстоће, што доводи у питање класичну дефиницију чврстоће материјала, којом се, до скоро, у уџбенцима наводило да не зависи од величине испитиваног узорка. У раду Т. Радетић разматрани су неки аспекти механизама формирања, раста и смањивања кристалних зрна.

Показало се да рачунарске методе, укључујући ту и прорачуне на бази првог принципа, представљају моћну алатку која омогућава истраживање система различитих комплексности, како на димензионој тако и на временској скали. Оне омогућавају и преглед великог броја система, што експериментално није изводљиво, као и разумевање општих трендова који су од великог значаја, како за теоретичаре тако и за експериментаторе. Коришћење овог концепта у примени металних и оксидних наночестица описане су у раду чији су аутори И. А. Пашти и сарадници.

Свесна значаја нанонаука и нанотехнологија, као и њиховог глобалног утицаја на човечанство, Српска академија наука и уметности је у јесен 2017. године покренула серију предавања посвећену овим темама, на основу којих је настала и ова монографија. Надамо се да ће ова монографија бити занимљива читаоцу и да ће моћи да послужи као мотивација за стварање прилика за истраживања онима који желе да сазнају нешто више о овим фасцинантним областима наука и технологија.

Велимир Р. Радмиловић
Српска академија наука и уметности

Џеф Т. М. ДеХосон
Краљевска холандска академија наука и уметности

ATOMISTIC AND CRYSTALLOGRAPHIC PHENOMENA DURING NANOGRAIN ISLAND SHRINKAGE

TAMARA RADETIĆ*

A b s t r a c t. - Nanocrystalline and ultrafine-grained metallic materials are considered to be interface-controlled as key factors in determining their unique properties are associated with grain boundaries. Due to the small size effect, atomic structure and mobility of grain boundaries have an important influence on the stability of a nanocrystalline structure. In this contribution, the phenomena related to the mechanism and kinetics of capillary driven grain boundary migration in thin Au films are reviewed. The shrinking of island grains in {110} and {111} mazed bicrystal thin films at elevated temperatures was observed by conventional and high-resolution *in situ* electron microscopy. Measurements of grain boundary anisotropy showed the preference for low index facets. Observed migration mechanisms of the facets involve collective motion of the atoms such as regrouping by atomic shuffles, glide and step migration. *In situ* HREM revealed that the facet migration is controlled by the nucleation and propagation of the steps/disconnections - by lateral motion as well as the propagation of buried steps perpendicular to the film surface. The erratic kinetic of grain shrinkage is consistent with migration mechanisms controlled by the step nucleation. Detailed analysis of the interfacial defects showed a range of step heights and dislocation contents. The step height limits the mobility of steps/disconnections in {110} films, while no such influence was observed in {111} films. There was no measurable grain rotation during the grain shrinkage.

Keywords: grain boundaries, interface facets, interface migration, capillarity, *in-situ* HREM

INTRODUCTION

It is well known that in polycrystalline materials, grain boundaries have an important influence on a number of material properties such as mechanical and electrical properties, corrosion resistance etc. The volume fraction of the grain boundaries increases exponentially in the microstructure of a new generation of structural materials such as nanocrystalline (grain size ≤ 100nm) and ultraf-

*Faculty of Technology and Metallurgy, University of Belgrade, Karnegijeva 4, Belgrade, Serbia; e-mail: <tradetic@tmf.bg.ac.rs >

ine-grained (grain size ≈100-1000nm) bulk metallic materials [1, 2]. These materials are considered to be interface-controlled as key factors in determining their unique properties are associated with grain boundaries [3, 4]. In nanocrystalline materials, capillary pressure or the driving force for curvature driven grain boundary migration, although of orders of magnitude smaller than, for example, driving force for recrystallization [5], becomes decisive for the stability of a nanocrystalline structure due to the small size effect [6, 7]. Hence, properties of grain boundaries, such as atomic structure and mobility gain additional significance. However, while there are a plenty of studies of structural aspect of grain boundaries, atomic mechanisms of grain boundary motion are far less understood.

A number of mechanisms for transfer of atoms across the interface has been proposed ranging from the motion of interfacial defects by climb and glide to uncorrelated atoms jumps by self-diffusion [5]. The migration mechanism and mobility is boundary specific and depends not only on the factors inherent to the structure of the boundary, but on a number extrinsic factors. Experimental studies of grain boundary migration at atomic scale are enormously complex due to a number of variables such as grain boundary geometry, thermodynamic and chemical aspects as well as the effect of surfaces and grain boundary grooves. In his pioneering work on direct observations of grain boundary migration on the atomic scale, Merkle [8-11] identified several mechanisms: grain boundary glide, collective rearrangements by atomic shuffles and motion of steps or disconnections [12] along the boundary.

This contribution gives a review of phenomena associated with dynamics of shrinking of circular, nanosized grains (~ 100 nm) under capillary forces in Au thin films. Study of the migration of grain boundaries in {110} and {111} mazed bicrystal films [13] covers behavior of the boundaries at opposite ends of coincidence lattice space [5]: low coincidence Σ99 and low energy Σ3 boundaries. Direct observations of grain boundary motion on the atomic scale by *in-situ* high-resolution electron microscopy at elevated temperatures and evaluation of mechanisms and kinetics of migration are of great importance to our understanding as well as predictive modeling of the behavior and design of advanced new materials [14, 15].

MAZED BICRYSTAL FILMS

Experimental studies of dynamics and mechanism of a grain boundary migration have to address a number of extrinsic and intrinsic parameters such as chemical segregations, surface effects, thermodynamics and crystallography of the interface, all of them having a strong influence on a grain boundary motion [5, 16]. Even with the elimination of the chemical effect by choosing model systems such as pure metals, the complexity persists since five parameters are describing grain boundary geometry – three to define misorientation and two for grain boundary plane or inclination [5]. Polycrystalline materials contain a network

of the various types of grain boundaries, so the dynamic study of such system would require knowing the geometric aspects of a spectrum of changing grain boundaries, rendering it an almost impossible task. The challenge to control and characterize grain boundary plane resulted in the oversight of the effect of the inclination on grain boundary energy and mobility in a number of studies [17–21]. However, recent computational studies [22] emphasized the significant effect of the inclination on grain boundary mobility.

An additional complication for the experimental studies of the grain boundaries at the atomic level is projection requirement that crystal lattices in both grains are on, preferably low index, zone axis reducing a range of grain boundaries suitable for the investigation to tilt and some special twist boundaries [8, 9, 23]. Various techniques of a bicrystal preparation have been employed to fabricate specimens that contain tilt grain boundaries, but most of them produced grain boundaries that cover small section misorientation/inclination space and characterization has been mostly confined to short segments of flat boundaries [24]. The method, based on physical vapor deposition growth of the heteroepitaxial metal thin films with multiple orientation variants on a single crystal substrate, was developed to provide fabrication of model grains with well-defined crystallographic parameters and geometry [13, 24]. Depending on the epitaxial relationship between the film and substrate it is possible to grow bicrystal, tricrystal or textured polycrystalline thin metal films [13]. The origin of the multiple variants is the lower symmetry of the thin film orientation with respect to the substrate orientation. This symmetry-breaking leads to formation of two or more variants in the film, with each variant equally probable since the substrate/thin film interface energies are degenerate for the variants. The resulting morphology is a polycrystalline film with the grains' orientations corresponding to variants' orientations.

Mazed bicrystals, polycrystalline structures with only two grain/variant orientations, are of special interest for the studies of dynamics of grain boundary migration. In conventional polycrystalline materials or, even, tricrystals grain boundary migration is affected by the presence of triple junctions and other geometric constraints that can act as pinning sites [25–27]. In mazed bicrystals, due to the absence of triple junctions, migration of grain boundaries is solely controlled by a grain boundary mobility. Morphology of a mazed bicrystal film resembles a jigsaw puzzle (Fig. 1), with grains having convoluted shapes with both concave and convex sections and a range of curvature [24, 28].

As a result, all grains have the same misorientation but boundary inclination is variable. The presence of a range of inclinations within a grain enables investigation not only of migration of a particular grain boundary plane but also interaction between different inclinations and its effect on grain boundary mobility and migration mechanism. Since grains/variants' surface energies are degenerate, the grain boundary migration in mazed bicrystal is driven by capillary forces leading to grain growth/shrinkage by eliminating grain boundaries of high curvature or unfavorable inclination.

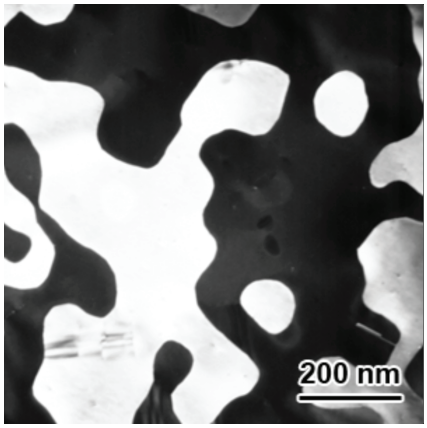

Figure 1. Typical mazed bicrystal morphology of {110} Au thin film. The dark field CTEM micrograph close to $<110>_{z.a.}$ shows the two variant orientations in black and white. The area fraction of grains in each variant is roughly the same.

{110} mazed bicrystal films were grown on single crystal {001} Ge substrates [13, 28]. The epitaxial relationship between the film and substrate defined as:

$$\{110\}_{Au} \,||\, \{001\}_{Ge} \text{ and } <\underline{1}10>_{Au} \,||\, <\underline{1}10>_{Ge}$$

The <110> two-fold symmetry axis of the film is parallel to the <001> 4-fold symmetry axis of the germanium substrate resulting in two equivalent variants in the film (Fig. 2a).

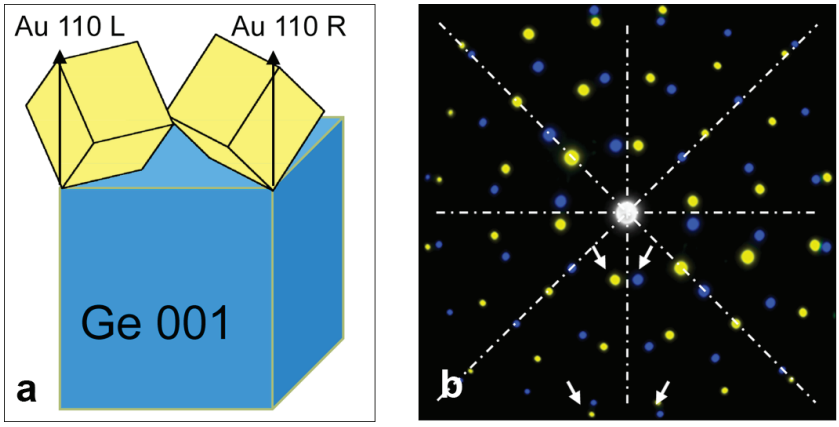

Figure 2. (a) Schematic presentation of the crystallographic relationship between two variants in {110} mazed bicrystal film Au thin film and {001} Ge substrate; (b) The bicrystal diffraction pattern shows the two orientations rotated 90° around common <110> axis. For clarity, diffractions spots corresponding to each variant are colored differently. Traces of mirror planes are outlined.

Two allowed grain orientations are related by a 90° rotation about the common <110> surface normal resulting in 4'mm' color symmetry group of the bicrystal as can be seen from the diffraction pattern in Fig. 2b. Characterization of the {110} mazed bicrystal film cross-section [29] showed that the grains are strictly columnar with grain boundaries perpendicular to the film surface, i.e. parallel to the <110> rotation axis. Hence, the crystallography of the grain boundaries is described by a Σ99 90° <110> tilt character. In this geometry, out of five macroscopic crystallographic parameters describing a general grain boundary, single is variable – one that defines grain boundary plane and it can vary from 0 to 2π.

{111} mazed bicrystal films were grown on a single crystal {111} Ge substrate [30]. The orientation relationship between two variants can be described by 60° rotation about the common <111> axis. The orientation relationship between the variants is not apparent from the diffraction pattern (zeroth order Laue zone) where it appears as a single crystal (Fig. 3a), since it is related to three-dimensional crystallography rather than to two-dimensional projection. Using the familiar notation of ABC stacking of close-packed {111} planes in f.c.c. crystals, one variant can be described as having ABC… and another ACB… stacking sequence (Fig. 3b). Such orientation relationship corresponds to the twinning operation, i.e. the interfaces between variants are Σ3 grain boundaries. The morphology of the film is more complex than in the {110} mazed bicrystals since grains are not strictly columnar. Majority of the boundaries are incoherent twin boundaries with {11$\underline{2}$} inclination that is parallel to the rotation axis. However, some of them do not penetrate through the film but are connected by short stretches of horizontal facets parallel to the standard {111} coherent twin plane [30, 31].

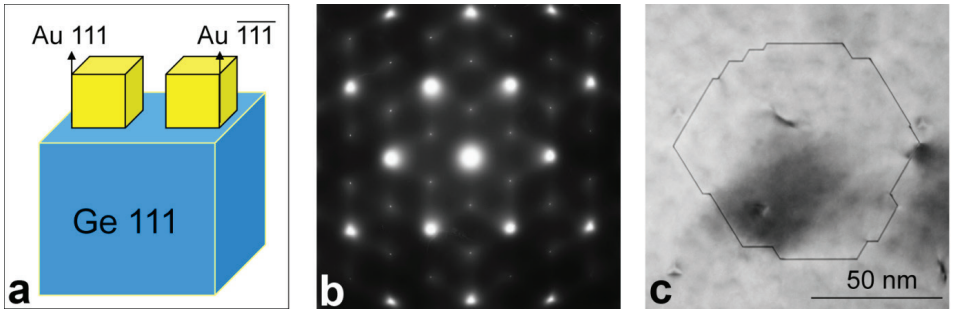

Figure 3. (a) Schematic presentation of the crystallographic relationship between two variants in {111} mazed bicrystal Au film and {111} Ge substrate; (b) The diffraction pattern of {111} mazed bicrystal thin film Au thin film does not reveal the existence of two variants. Terminal (forbidden) 1/3<42$\underline{2}$> reflections are observed in the pattern; (c) Bright field image close to $<111>_{z.a}$. of polygonal, strongly faceted grain.

<110> mazed bicrystals

S h r i n k i n g o f t h e i s l a n d g r a i n. – During thermal annealing, a grain boundary migration is mazed bicrystal films is driven by capillary

forces. The grain boundaries of high curvature or unfavorable inclination are eliminated. In small, isolated, fully convex island-like grains (Fig. 1) grain boundary moves toward the center of curvature causing shrinking of the grain until the grain annihilation. Well defined geometry and topology of the fully convex grains made the suitable for investigation of a number of phenomena and effects taking place during the grain shrinkage.

Since grain boundary migration is a dynamic process, the primary interest is to establish whether grain boundaries preserve tilt character during the grain shrinkage. Following the Mullins analysis [32], the expectation was that the grain would adopt a catenoid shape during the contraction. Catenoid is zero-mean-curvature shape resembling the hour-glass; grain boundaries should adopt such shape under influence of capillary forces acting at the triple points at the surfaces in an isotropic grain when the grain diameter approaches a thickness of the film. However, the experimental results on shrinkage of island grains in {110} mazed bicrystals films showed that the grain boundaries preserve tilt character as they move. An example of the final stages of an island grain shrinkage is presented in Fig. 4 [33]. The image sequence corresponds to the frames from the *in situ* recording with TV rate (30 frames/s). The specimen is tilted for a large angle providing the three-dimensional visualization of the cylindrical shape of the island grain. It is clear that the grain remains cylindrical until the last 33ms. In contrast to {110} Au films, the adoption of the catenoid shape was observed during island grain shrinkage in Al films by Mompiou et al. [34]. The difference in behavior of island grains in Au and Al films is likely to be related to the strong anisotropy of <110> grain boundaries in Au. The anisotropy and strong tendency of <110> grain boundaries to preserve tilt character was also observed during the retraction of the Ge wedge in contact with the mazed bicrystal Au film leading to grain boundary drag and abnormal grain growth [29].

The important consequence of preservation of the cylindrical shape is that, since the grain boundaries remain parallel to the <110> rotation axis and preserve tilt character, the grain shape evolution can be completely described by its projection along the tilt axis reducing the three-dimensional problem to two-dimensions. Additionally, preservation of the grain boundary tilt character enables HREM observations of the atomic structure of the boundaries.

The last image in the sequence in Fig. 4 shows that the grain annihilation leaves behind dislocations. Numerous recordings of a grain shrinkage [33] showed that annihilation inevitably leaves dislocation debris behind, but there is no unique dislocation configuration and the number and arrangement of dislocations varies with each experiment. An illustration of a different dislocation configuration left after the shrinkage is shown in Fig. 5. The foil is tilted about 20° around $\mathbf{g}=(200)_{l}\|(022)_{\mu}$ to ensure that grains of both variants are in diffracting condition so the grain boundaries are visible through the fringe contrast.

During *in situ* annealing at 310°C, the smallest grain, less than 100nm in diameter, shrinks and disappears while larger grains remain immobile. In this

case, as in others, high dislocation mobility and their tendency to be annihilated at surfaces prevented detailed characterization and Burgers vector determination of the debris.

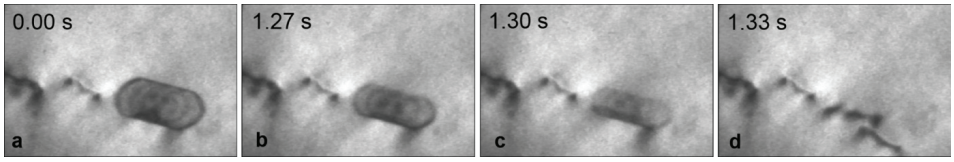

Figure 4. The sequence of images from an is situ TV rate video recording showing final stages of the grain shrinkage at 311°C. The foil was tilted ≈20° around $\mathbf{g}=(220)_{\lambda}/(002)_{\mu}$, so cylindrical shape of the grain is outlined by grain boundary fringes. The collapse of the grain leaves behind two dislocations. (from T. Radetic et al, Acta Mater. 60 (2012) 7051–7063[33])

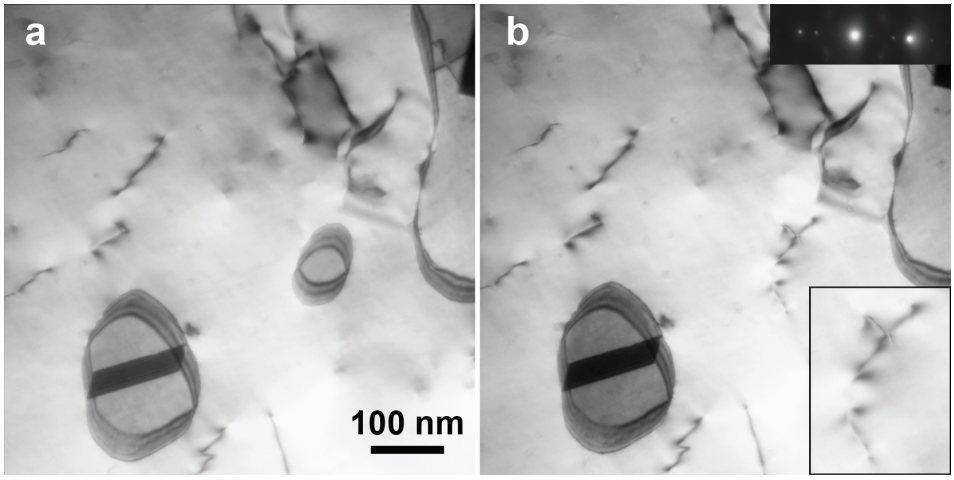

Figure 5. Leaving behind dislocation debris is characteristic of island grain shrinkage, although dislocation content and configuration varies. Bright field images (a) before and (b) after shrinkage show an example of dislocation debris ($\mathbf{g}=(220)_{\lambda}/(002)_{\mu}$ is about 20° from foil normal).

Analysis of high-resolution images by the construction of a Burgers circuit around a grain at different stages of shrinking and after the final collapse allowed for a partial characterization of the dislocation debris. The limitation of HREM imaging in the dislocation characterization is that only edge components of dislocations with line direction perpendicular to the image plane can be characterized, i.e. components whose Burgers vector is parallel to the imaging plane. Fig. 6 shows frames extracted from *in situ* HREM recording of the shrinking island grain. The dislocation arrangement after the grain annihilation is complex

and consists of extended dislocation and a defect (Fig. 6c). The Burgers circuit construction gives a closure in the failure of ¼<112> corresponding to the edge component of 60° dislocation. Same closure failure was found following the construction of a Burgers circuit around the grain before collapse (Fig. 6a-b) indicating that the grain boundaries contain extrinsic dislocations. Although it cannot be assumed that the mechanism of migration is identical for free-standing films and films still attached to the substrate, similar conclusions were drowned from the observations made during the shrinkage of an Au grain on Ge substrate [33]. Using moiré fringes, formed by interference of $\{200\}_{Au}$ and $\{220\}_{Ge}$ reflections [29], to magnify any defect in the film, extra planes corresponding to dislocations were visualized and the Burgers circuit showed same closure failure before and after the grain shrinkage [33].

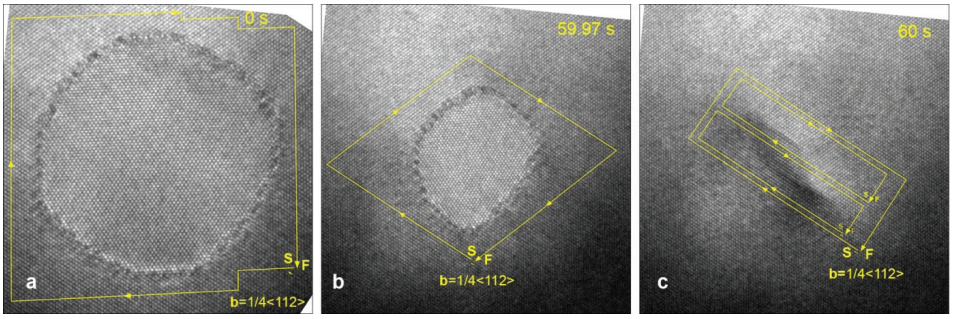

Figure 6. The sequence of HREM images recorded *in situ* at 206°C showing grain 60s, the single frame before shrinkage and dislocation configuration immediately after the collapse. Burgers circuit constructions around the grain and defects show the same net dislocation content. Following the lattice fringes during the grain contraction revealed the absence of grain rotation.

The dislocation debris after grain shrinkage is also found in the MD simulations [33]. Similarly to experimental observations, the MD simulations showed that the dislocation configurations left after the grain annihilation vary from one grain to another. However, the simulations gave the net Burgers vector of the dislocation configurations zero which was not the case for the experiments.

Preservation of the cylindrical shape of island grains through the shrinkage provided a model system for testing the concept of coupling of the grain boundary migration and shear displacement followed by a rotation of the island grain. According to Chan and Taylor theoretical framework [35], the rotation of an isolated grain can be induced by grain boundary migration due to the coupling of grain boundary motion in the normal direction and tangential translation of adjacent grains due to the lattice shear independently of a driving force. Based on the framework, a number of molecular dynamics simulations and phase-field modeling showed a clear evidence of shear-migration coupling and grain rotation of

different grain boundary types [36-42]. While experiments validated simulations on the shear-migration coupling of planar boundaries [43], experimental evidence for the rotation has been less clear. A grain rotation in fiber textured thin films [44,45] has been observed, but no correlation between misorientation, stress and rotation has been made. Experiments on mixed tilt/twist boundary in Al showed definite grain rotation, along with boundary migration under applied shear stress [41], however there was no evidence of grain rotation during *in situ* observations of shrinking island grains in Au [46] and Al bicrystal [47] and tricrystal thin films [34]. Series of high-resolution *in situ* heating experiments on shrinking of a number of island grains in {110} Au mazed bicrystal films recorded by TV rate camera showed unequivocally that the misorientation between the island grain and surrounding grain did not change throughout the shrinkage within a temporal resolution limit (33 ms) [33]. No measurable grain rotation was observed until the last frame before complete collapse (Fig. 5). The similar result was produced by MD simulations [33].

The absence of grain rotation during shrinkage is likely to be due to the thermodynamic factors since grains rotate toward the low energy misorientations in order to decrease the integrated interfacial free energy of the island. A 90° <110> bicrystal has high 4'mm' symmetry and hence is located at a symmetry-dictated minimum for which the driving force for grain rotation - $d\gamma/d\theta$ is zero [33]. Early work of Babcock and Balluffi and [46] showed that, during island grain shrinking under capillary forces, grain boundary moved erratically without producing shear deformation. However, their study was on low coincidence site lattice $\Sigma 5$ grain boundaries in which grain boundary migration was conducted by lateral motion of pure steps [12, 48, 49]. In the case of $\Sigma 99$ grain boundaries, while pure steps have been observed, as will be discussed later, grain boundary migration was carried out by the lateral motion of defects with a step and dislocation character, i.e. disconnections [12, 49], so net shear has been expected.

Measurements of grain boundary migration rate (Fig. 7) showed that it was not constant and did not obey parabolic dependence of migration kinetics expected for capillary pressure driven process [5].

The grain contraction alternates between long intervals of inactivity and faster events. When the grains diameter reaches a critical size 25-30nm the rate of shrinkage suddenly accelerates. The erratic migration, occasional rapid movements followed by periods of stagnation, is characteristic of migration kinetics controlled by the energy barrier for step and kink nucleation on faceted interfaces [5, 46].

G r a i n b o u n d a r y m o r p h o l o g y. – If the grain boundary energy is isotropic, all inclination orientations would occur with an equal probability at equilibrium and the grain would have the spherical shape. The cylindrical grain shape and a strong preference for the tilt boundaries in the {110} Au mazed bicrystal [33] are, per se, a mark of anisotropy. Additionally, deviation from randomly curved boundaries in the film plane is a sign of faceting or preference for certain boundary inclinations of tilt boundaries in the mazed bicrystal. The grain

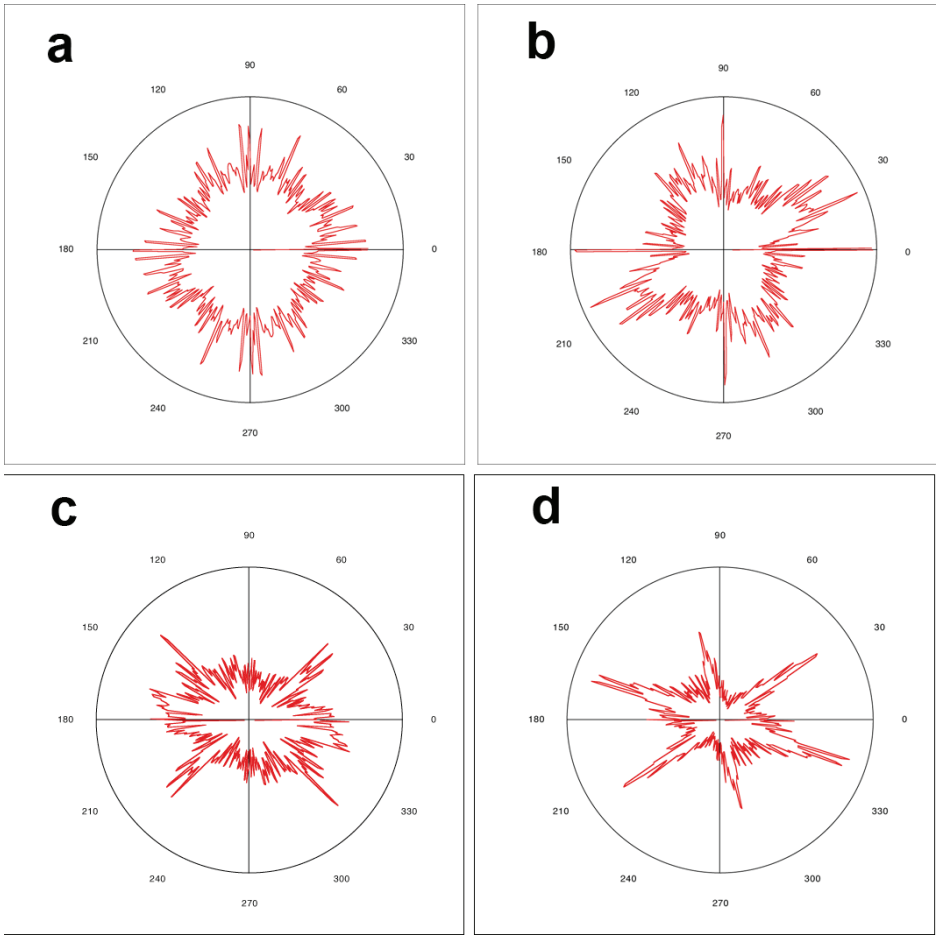

Figure 7. Rose plots of {110} (a, b) and {111} (b, c) Au mazed bicrystal films. The anisotropy of {111} bicrystals is much more pronounced. There is an increase in anisotropy after annealing 20min at 340°C (b, d) with respect to the as-deposited state (a, c) for both types of bicrystal films.

shape or preference for certain planes can be quantified by the rose plot, a polar histogram of total interface length as a function of orientation [50]. In isotropic case the rose plot is a circle. Systematic deviations from the circular shape, manifested through the presence of lobes in the plot, indicate anisotropy – that the grain boundary energy is a function of inclination [51] or kinetic parameter, i.e. a difference in grain boundary mobility when the grain boundary migration is involved. The anisotropy parameter, defined as the ratio of the boundary area in faceted orientation to the total boundary area, changes from 0 for an isotropic case to 1 for completely faceted. This measure is independent on of the scale or topography of microstructure, i.e. it applies equally well to large complex jigsaw-puzzle

shaped grains as to fully convex island grains. From the rose plot anisotropy, it is possible to determine on a mesoscopic scale which boundaries are significant and focus on them for further structural characterization on a microscopic scale.

In the case of {110} Au bicrystals, there is a measurable degree of anisotropy in as-deposited state [28, 33]. Deviation of the plot from the perfect circle increases with annealing (Fig. 8) since boundaries with high energy and/or high mobility inclinations grow out of existence during grain coarsening. From the rose plot data shown in Fig. 8a-b, the anisotropy parameter was found to increase from 0.37 in as-deposited state to 0.62 after annealing [28], indicating evolution of preferential grain boundary inclinations. However, the anisotropy degree is smaller than observed in other mazed bicrystal systems such as platinum on (0001) sapphire [52], aluminum on {100} Si [24] and Au on {111} Ge (Fig. 8c-d). Smaller anisotropy parameter and broad lobes are due to the micro-faceting and step formation causing deviation of an average grain boundary plane from the actual orientation of microfacets which are only visible at a higher resolution. The rose plot anisotropy is much more evident when the high-resolution images are characterized [53].

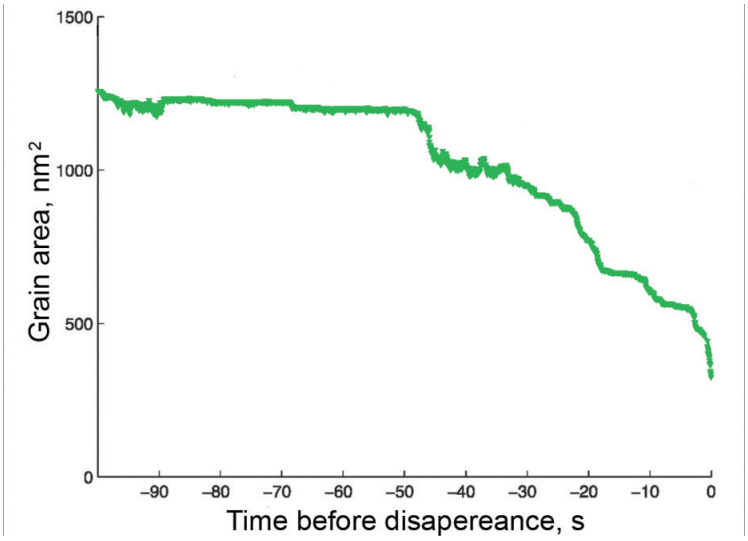

Figure 8. A typical curve of a change in the grain area with time during annealing at 290°C showing erratic shrinkage kinetics [33].

In situ conventional TEM experiments showed that certain boundary segments are entirely eliminated and a facet coarsening takes place during annealing. The resulting microstructure is increasingly dominated by a small number of preferred facets, whether individual grains have complex, convoluted shape or are convex island grains. Correlation between the rose plot and corresponding diffraction pattern revealed that the peaks in the rose plot correspond to the mirror planes of the bicrystal [33].

High-resolution electron microscopy (HREM) micrographs exposed clear tendency of grains toward faceting on three characteristic planes, denoted A, B, and C:

A-facet:	$(\underline{1}1\sqrt{2})_{\lambda} \mid (1\underline{1}\sqrt{2})_{m}$	multiplicity 4
B-facet:	$(1\underline{1}1)_{\lambda} \mid (1\underline{1}2)_{\mu}$	multiplicity 8
C-facet:	$(00\underline{1})_{\lambda} \mid (1\underline{1}0)_{m}$	multiplicity 4

Because of 4'mm' symmetry of the bicrystal [13], each of these facet types has different crystallographically equivalent variants, so the equilibrium Wulff shape of the island grain would be bounded by 16 facets. Although the anisotropy plots show a range of inclinations, the most of them are vicinal inclinations comprised of micro-facets and steps. The facets, actually, tend to form sharp junctions (Fig. 9).

The facet A (Fig. 9) is symmetrical grain boundary and, as it is generally the case for symmetrical tilt boundaries, it is parallel to the mirror plane of the bicrystal. The atomic arrangement resembles symmetrical boundary observed in Al {110} mazed bicrystal films whose structure has been investigated in detail [24, 54]. The periodic atomic relaxation into structural units with a short repeat distance has been observed. The A facet tends to be short with small steps between segments of structural units. The step defects are introduced to accommodate strain due to deviations from exact 90° misorientation; the boundary is actually parallel to rational {557} planes of the bicrystal requiring adjustment of ±0.6 from 90° misorientation, corresponding to rational Σ99 89.4° or Σ99 90.6° boundaries. Only through this small deviation from exact 90° misorientation the boundary can become periodic with a short repeat distance.

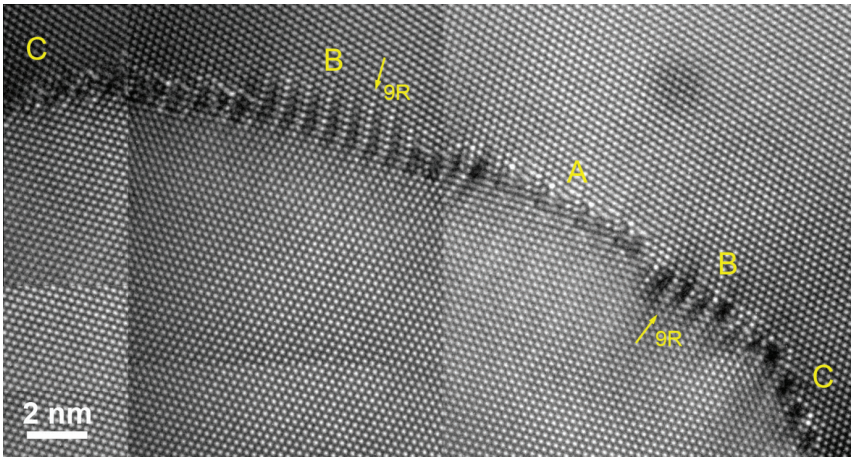

Figure 9. Composite high-resolution image of a grain boundary section of an island grain showing three major facets/inclinations. The image also illustrates 9R dissociation at B-facets.

This facet is less prominent than the facets B and C in Au films [33] in contrast to Al {110} mazed bicrystal films where the symmetrical boundary is the most frequently found facet [24].

According to the equilibrium Wulff shape, A- facet is nested between two symmetry-related B- facets (Fig. 9). The most remarkable feature of B- facet is its wide structure – the presence of narrow, about 1 nm thick, slab of the dissociated boundary. Closer inspection of the HREM micrographs reveals contrast modulations associated with intrinsic stacking faults (Fig. 9). Another important feature is that as $(1\underline{1}1)$ lattice fringes approach the boundary from the {112} grain side they bend for about 4-7° until reaching corresponding planes in {111} grain. The continuity of the close-packed {111} planes is maintained across the interface except for the occasional steps that accommodate for incommensurate crystallography of misorientation [55].

Computational simulations [56, 57], as well as experimental observations [58-60], showed that in low stacking fault metals such as Au and Cu, both symmetrical and asymmetrical boundaries have a tendency to relax by the emission of stacking faults in a regular manner into one or both grains. The stacking faults terminate in partial dislocations that create low angle grain boundary, while dissociated slab adopts f.c.c. based long-period structure consisting of intrinsic stacking faults. Detailed analysis of atomic structure coupled with MD simulation of the B-facet, i.e. $(1\underline{1}1)_{|}|(21\underline{1})_{\mu}$ boundary in Au by Medlin et al. [59] showed that the dissociated region has 9R structure. In the 9R structure, on every third close-packed {111} plane intrinsic stacking fault is generated resulting in ABC|BCA|CAB… stacking sequence. Such grain boundary geometry can be described in terms of Shockley partial dislocations: the periodic unit of the boundary consists of six {111} planes with a partial dislocation on each plane [59]. Among the total of six Shockley partials assigned to the periodic unit four are 90° and two are 30° partial dislocation in a $\perp_{90°}|\perp_{90°}|\perp_{30°}|\perp_{90°}|\perp_{90°}|\perp_{30}$ sequence. The 30° dislocations separate producing the extended configuration and intrinsic stacking fault on every third plane and 9R structure.

Although it does not lie on any of mirror planes, the bicrystal symmetry renders the B- facet boundary to have the high multiplicity of eight. Fig. 9 shows that two B facets, $(1\underline{1}1)_{|}|\ (21\underline{1})_{\mu}$ and $(1\underline{1}1)_{|}|(21\underline{1})_{\mu}$, border symmetrical boundary. Their dissociation on opposite sides of the grain boundary, one outside and the other inside the island grain, might have important consequences for the observed asymmetry of grain boundary migration.

Results of the rose plot analysis indicate that the preferred facet is C- or asymmetrical $\{110\}_{|}|\{100\}_{\mu}$ grain boundary (Fig. 9). This boundary has been previously studied by high-resolution electron microscopy and atomic simulations [61-63]. At C- facet (001) planes of one grain and (110) planes from the other grain meet at the interface (Fig. 10).

Hence, while there is a perfect match along the <110> tilt axis, the ratio of interplanar spacing in the direction perpendicular to the axis is irrational, $1/\sqrt{2}$, so the boundary is incommensurate in one direction. The key features of this in-

terface are pentagonal structural units distributed quasi-periodically along the interface [63], tendency to form steps of certain height [53] and chevron defect reconstruction at the triple junction with the surface [62, 64]. While consequence of quasi-periodicity is an ability of two crystals at the interface for a frictionless glide along incommensurate direction [65], steps and chevron defect have an important role in the interface migration, acting as a vehicle for grain migration and as eventual pinning site similar to the surface grooves [32], respectively.

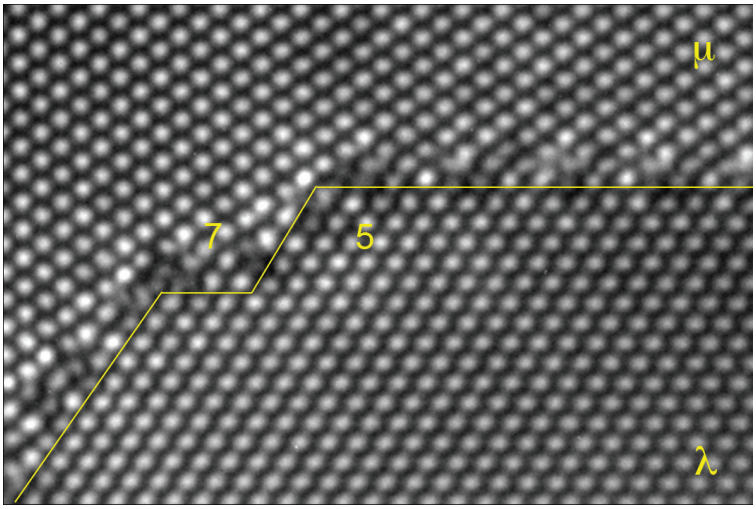

Figure 10. HREM image of C-facet or asymmetrical 90°<110> (110)|(001) tilt grain boundary. This boundary lies along the mirror plane of the bicrystal. Due to the incommensurate spacing of lattice planes at the interface the boundary is quasi-periodic. There is 7|5 step close to the facet junction.

High-resolution images showed that a number of characterized C- facets contain step-like defects resulting in the average inclination of the boundaries a slightly off C– plane and giving rise to lobes instead of sharp peaks in the rose plot [53]. An example of the step-like defect is shown in Fig. 10. The step height has been denoted as *n*|*m* where n and m are the numbers of {100} and {011} planes in the two grains ending at the step. The step in Fig. 10 is a 5|7 step where 5 {100} planes in λ meet 7 {011} planes in μ.

To characterize the behavior of the steps in $(100)_{\lambda}|(011)_{\mu}$ boundaries, heights of over hundred steps in the facets of island grains were measured. These measurements showed steps heights ranging from 1|1 to 7|10. If the strain minimization is only criteria, i.e. the smallest Burgers vector associated with the disconnections, the preferable step height would be, not the most frequently observed, 5|7 which is characterized by a mismatch of only 1%. Majority of the observed steps are of type 2|3, 3|4 or 4|6, for which the rational ratio of n:m approximates the irrational ratio of interplanar spacing of {100} and {110} planes, n|m=1|√2, within 6%. The mismatch

between step height in two grains results in a gap that has dislocation character and can be characterized by a Burgers vector. Following the Hirth-Pond treatment of interfacial defects [12, 49], those steps which have dislocation content are classified as disconnections, while pure step corresponds to a step height 5|7, which, as the closest approximant of n|m=1|√2, has essentially zero dislocation content.

It is important to note that if *n* and *m* have different parity, A-B stacking of the crystal planes in the direction parallel to the tilt axis would be changed on one side of the step to A-A or B-B stacking on the other side of the step. In order to avoid such energetically unfavorable configuration, an introduction of dislocation with a screw component with ***b***=¼<110> parallel to the axis into the disconnection interface is required [53].

G r a i n B o u n d a r y M i g r a t i o n. – The experimental observations highlighted the importance of the irrational orientation relationship not only for the atomic structure of facets but its role in the grain boundary motion.

High-resolution recordings of shrinkage of entire grain during *in situ* annealing showed that C-facets are dominant and that the rate of the island grain shrinkage is controlled by their mobility [33, 53]. It has been observed that C- facets have a tendency to remain flat and stationary while adjoining inclined facets advance at more regular steady pace. Such behavior is illustrated in the first two frames of the image sequence in Fig. 11.

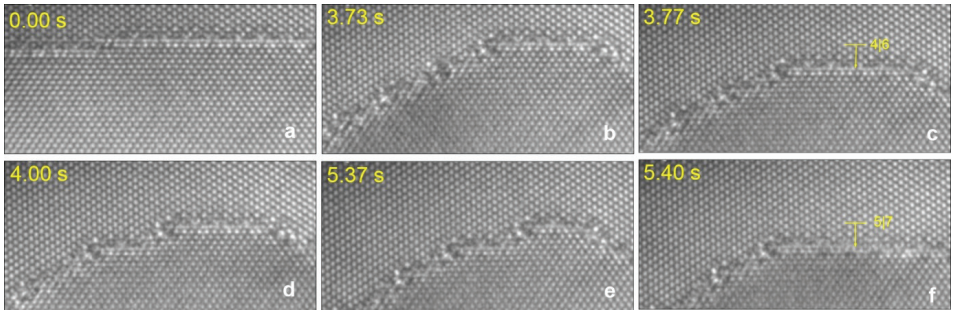

Figure 11. The sequence of images from *in situ* experiment recorded with TV rate showing the migration of C-facet. Initially static C-facet, after reaching some critical width by the encroachment of neighboring facets, moves perpendicularly to itself by jumps of 4|6 or 5|7 {001}|{110} lattice spacing (T=206 °C).

The C- facet was stationary for several minutes but then it suddenly advanced after reaching a critical width due to encroachment (Fig. 11c). The sudden movement corresponds to the jump length of 6{110} planes in the upper crystal and 4 {100} planes in the lower crystal as indicated by the reference line. Once activated, the facet can exhibit a cascade of several jumps, one among them shown in Fig. 11e-f. Characterization of successive positions before and after the jump for a large number of facets showed that there is a preferred jump distance, i.e. C- facet tends to move by discrete jumps of 7|5 or 6|4, while the critical width of C- facet before triggering the jumps is in the range 4-12 {110} interplanar spacing.

The occurrence of the jumps within 33ms (Fig. 11b-c and 11e-f), i.e. within a single frame of TV rate recordings, highlights the significance of temporal resolution in addition to the spatial one for *in situ* experiments. Recent advances in instrumentation have made it possible to extend the range of temporal resolution of such observations [66]. Gatan K2-IS direct electron detection camera with an imaging rate of 400 frames per second (2.5 ms per frame) provided a more detailed insight in the mechanism of the C- facet migration (Fig. 12). The appearance of moiré pattern in the internment frames between the beginning and the end of the jump (Fig. 12b-d) reveals the occurrence of overlap between two grains during the interface migration and indicates that the jump proceeds by formation and progression of a step parallel to the film surface. Since the step is along the axis of projection, its progression can be observed only indirectly through the changing moiré fringe contrast (Fig. 12b-d) as the facet progresses from the initial (Fig. 12a) to the final position (Fig. 12e). The imaging technique limits the knowledge of the topology of the buried step – whether is it single step, inclined, double kink and whether it originates at the surface.

There is a number of observations that a grain during shrinkage becomes elongated indicating the asymmetry in the mobility of C-facets [33]. The facets move more readily inward if the island grain planes terminate on a (011) righter than on a (100) plane. This effect has important implications for interface mobility which is usually assumed to be independent of the direction of motion. In addition to the described interface migration through the jumps initiated by a formation of buried steps, another mechanism of the C-facet migration is via lateral motion of disconnections and steps (Fig. 13). The disconnections with a small step height such as 1|2 and 2|3 have greater mobility than those with higher steps like 4|6 or pure step, 5|7. One of the characteristics of highly mobile disconnections is odd|even parity of the step height that implies the presence of a screw dislocation in the direction normal to the surface of the film. The presence of both edge and screw dislocation components in disconnection implies quite complex motion involving both dislocation climb and glide.

The disconnections with $m|n \leq 2|3$ on a long facet tend to fluctuate back and forth along the facet. The fact, that such defects can be considered to have zero curvature because there is no change in the grain boundary area as long as they move along the facet [67], suggest that other factors like elastic interactions play role in their motion. Similarly to the jumps of C- facet perpendicularly to itself, for steps with $m|n \leq 2|3$, the frequency of jumps is so high to be characterized accurately at the rate of TV recording. Using a Gatan K2-IS direct electron detection camera it became possible to track the random fluctuations of such steps and extract their mobility [68, 69]. The statistical analysis of the amplitude of fluctuations showed the involvement of discrete increments and preference for jump length of 2|3, 3|4 or 5|7 in the lateral direction. Clearly, all of the jumps being an approximation of $\sqrt{2}$ within 6% point out that despite the grain boundary incommensurate character there are preferred sites for triggering or arresting a step motion.

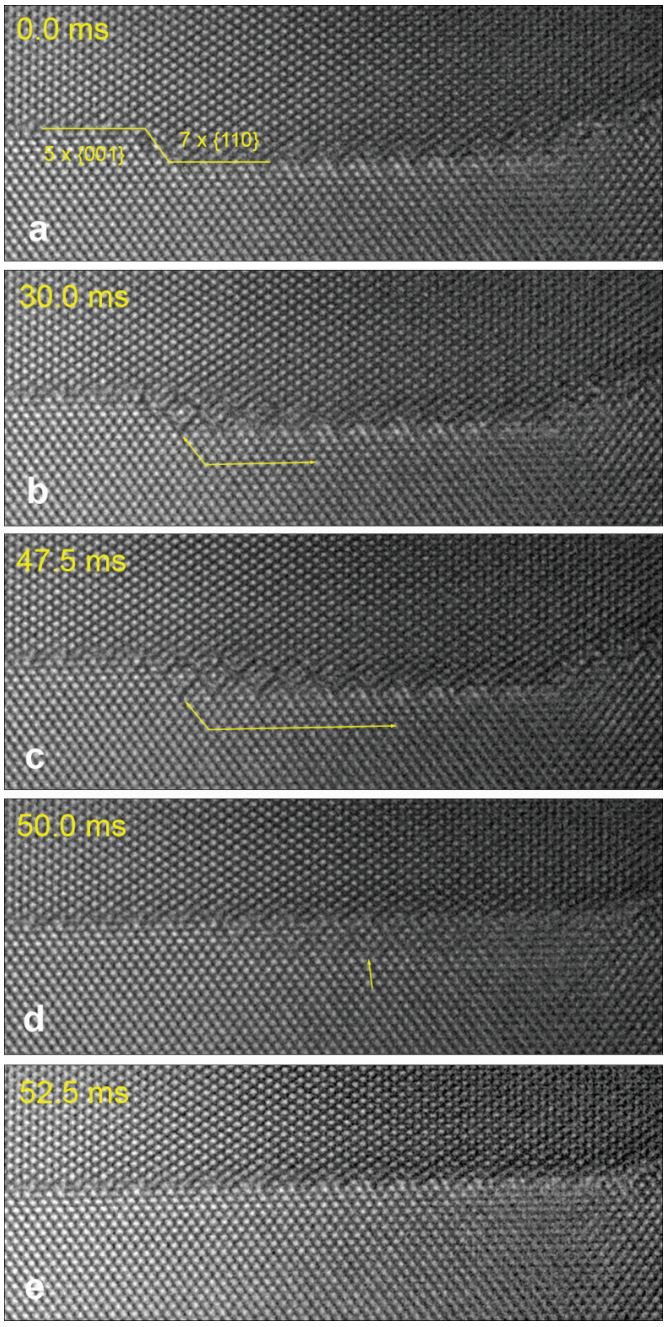

Figure 12. The sequence of images recorded with Gatan K2-IS direct electron detection camera. High recording rate reveals moiré fringes that indicate that the C-facet "jump" mechanism involves the creation of a buried step (T=210 °C).

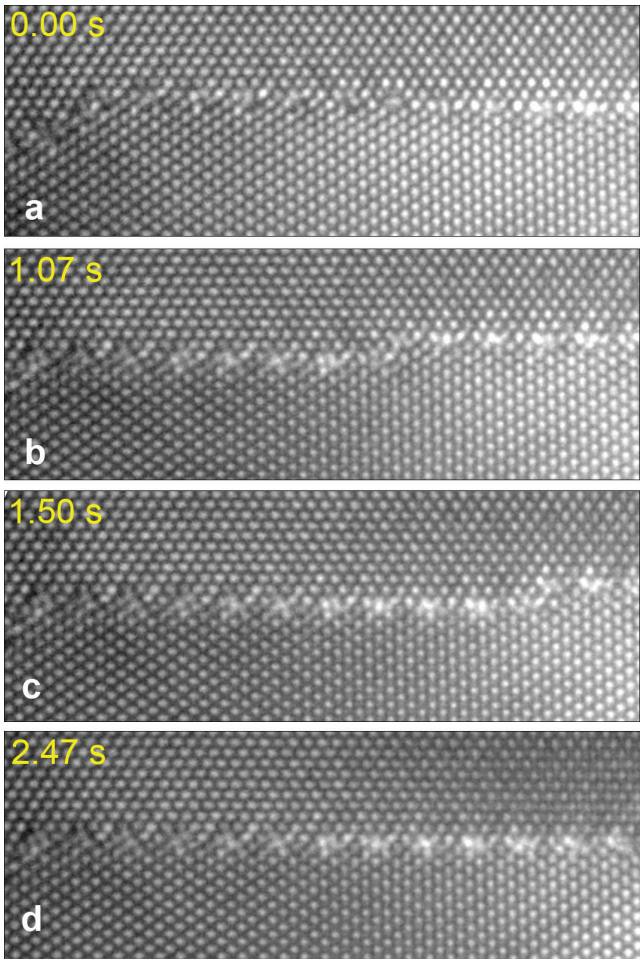

Figure 13. Lateral propagation of a 2|3 step along the C-facet recorded with TV rate camera (T=206 °C).

The steps nucleate heterogeneously with preferential sites being facet junctions. Disconnections with a height 1|2 forms at a junction of C- and B- facets by what is suggested to be some kind of pole mechanism [34, 70]. Small disconnections are produced in an avalanche and move along the facet. Sometimes, disconnection with lager step height swipes the facet in the reverse direction. Disconnections lateral motion in both directions along the interface contributes to the island grain shrinking, and the glide of disconnections of opposite sign might be the cause of cancellation of their dislocation content, in lieu with observations constant net dislocation content during the island grain shrinking.

Righter than only by the strain level, the step height appears to be influenced by the structure of adjacent facets. Most of the facet junctions connect C- to

dissociated B- facets (Fig. 8) and the observed step heights can be directly correlated to the geometry of the 9R structure [55, 59]. The periodic unit of the B- facets, consisting of six {111} planes with a partial dislocation on each of them, includes six layers of {110} planes on {111} side of the B facet and 4 layers of the {001} planes on {112} side. 4|6 ratio corresponds to one of the more frequently observed steps on C- facet. The partial dislocations are regularly distributed on {111} planes, so the periodic unit of B-facet contains two subunits each containing two 90° and one 30° Shockley partial. Separation of one subunit from the B-interface and its lateral glide on C- facet leads to the formation of the most frequently observed, very mobile, 2|3 disconnection. Additionally, 9R dissociation includes a rigid shift of ⅛<110> [59] that might facilitate nucleation of the screw dislocation at the junction necessary for the steps of different parity.

Although C-A facet junctions do not represent equilibrium junctions according to the Wulff shape of an island grain and bicrystal symmetry, they do occur (Fig. 14). Periodic unit of A- facet corresponds to seven layers of {110} planes and five layers of {110} planes and, similarly to C-B junctions, separation of a periodic unit from the rest of the facet can lead to the formation of a 5|7 pure step (Fig. 10). The range of observed step heights is a product of recombination of disconnections, their coalescence or partial annihilation [71].

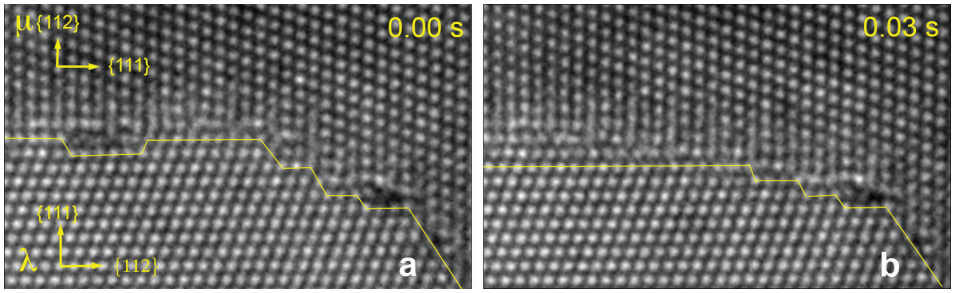

Figure 14. Migration of B-facet or {111}|{112} inclination by glide along continual {111} planes. As it moves, facet drags dissociated section behind.

Facets A- and B- show more regular migration rate than C-facets during the island grain shrinking. Relaxation of B- facets into a 9R configuration provides continuity of {111} planes across the interface. Such dissociated grain boundaries may be highly mobile [8]. Observations of the migration of B-facet indicate that it moves by a glide while extended boundary is dragged behind maintaining the width of dissociated slab constant (Fig. 14). The B-facets contain steps necessary to accommodate of incommensurate misorientation (Fig. 14), Although analysis by Pond and Medlin [55, 72] showed that the steps on B- facets have also dislocation character and that the disconnection glide is expected, no lateral motion of steps on these facets have been observed.

Migration of A- facets or symmetrical boundaries takes place by a cooperative motion of grain boundary segments (Fig. 15) that tend to correspond to

the periodic unit of the symmetrical boundary. In addition to advancing toward the center of curvature of the island grain, fluctuations of the segments back and forth involving reversible reshuffling have been observed. Apparently, all of the observed processes during the migration of the grain boundaries are collective phenomena involving coordinated regrouping and shuffling of a large number of atoms [8].

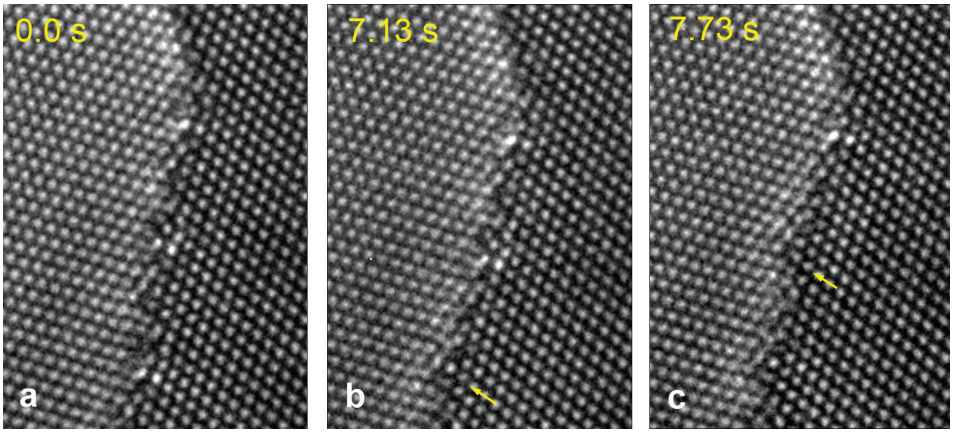

Figure 15. Migration of A-facet or symmetrical grain boundary. In order to accommodate for deviation from an exact orientation, the boundary is frequently segmented with steps between sections. Migration involves coordinated motion of the atoms in the segments. Arrows show the position of the bright pair of spots before migration.

Shrinking of the island grain in {111} mazed bicrystal films. – The grain boundaries in <111> mazed bicrystal films exhibit a much greater degree of anisotropy compared to <110> mazed bicrystals (Fig. 7). Even in as-deposited state, the microstructure is composed of strongly faceted grains in two twin-related orientational variants. The majority of grain boundaries are incoherent Σ3 twin boundaries perpendicular to the film surface with low energy {11$\underline{2}$} inclination [22]. There are three {11$\underline{2}$} facets running parallel to the <111> rotation axis and, at facet junction, they meet at 120° angle (Fig. 16a), so the grain shape of an island grain approximates hexagon (Fig. 3c). The grain boundaries are frequently broken into smaller facets giving an appearance of saw-tooth morphology (Fig. 16b). The length scale of the steps is much coarser than in the case of {110} mazed bicrystals, so in order to get a broader view of grain boundary, imaging with so-called "forbidden" or "terminal" 1/3{422} reflections [73, 74] was applied. Such imaging allowed to trace grain boundaries on the mesoscopic scale and to cover greater migration distances.

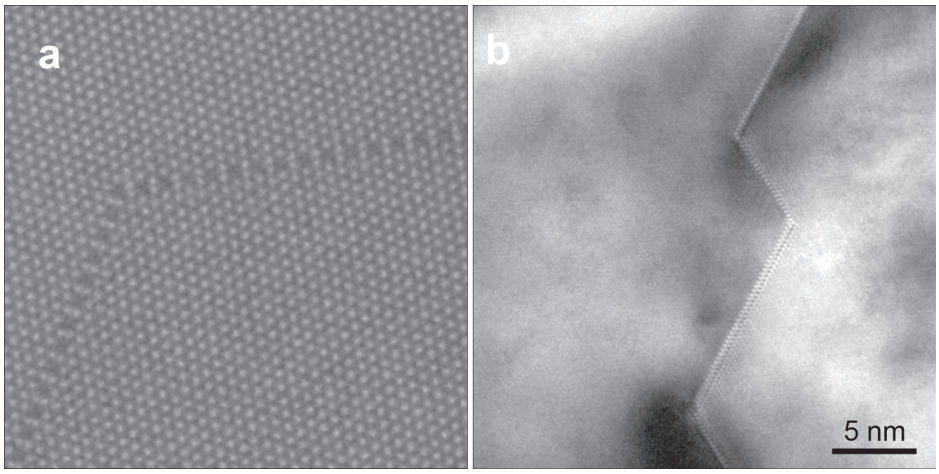

Figure 16. (a) STEM image of a facet junction in a {111} mazed bicrystal grains; (b) Grain boundary in {111} Au film imagined using terminal reflections. At the facet junctions, there is a change in contrast indicating the presence of dislocations, in agreement with previous conventional TEM observations [3].

The shrinkage of {111} island grains starts with the coalesce and annihilation of steps, a mechanism analog to one reported in CTEM study of facet coarsening by Medlin et al. [75]. The steps interactions are righter quick and can have a high degree of complexity as the reaction may involve multiple steps (Fig. 16). In contrast to the {110} bicrystals, where the steps of height over few atomic layers are mostly stationary, in <111> bicrystals step height does not appear to affect mobility significantly. Due to the high symmetry of misorientation and equivalency of the planes meeting at the junction, lateral motion of a step can take place along either of facets. Similarly, the fluctuation of steps along a longer facet is not limited by the step height. Fig. 17 illustrates simultaneous fluctuation of two steps with height over ten atomic spacing. The fluctuation frequency is so high that even high recording rate of 2.5 ms per frame is not sufficient to isolate individual events (Fig. 18).

Once the steps are eliminated and an island grain adopts smooth polygonal shape (Fig. 19a), the grain can become remarkably stable and resistant to shrinkage for a periods time whose length can extend to tens of minutes up to a few hours. However, at some point, the motion of a whole facet can be triggered initiating the rapid shrinking. Such behavior is illustrated in the image sequence of shrinkage of the grain with a shape of almost perfect hexagon (Fig. 19). Recent simulations of migration of flat and stepped boundaries showed that the migration is controlled by the nucleation of islands or double kinks [76, 77]. In a number of observations of a whole facet migration no step formation in the imaging plane was detected, suggesting that the buried steps have a role in triggering the motion as in the case of C-facets of <110> island grains.

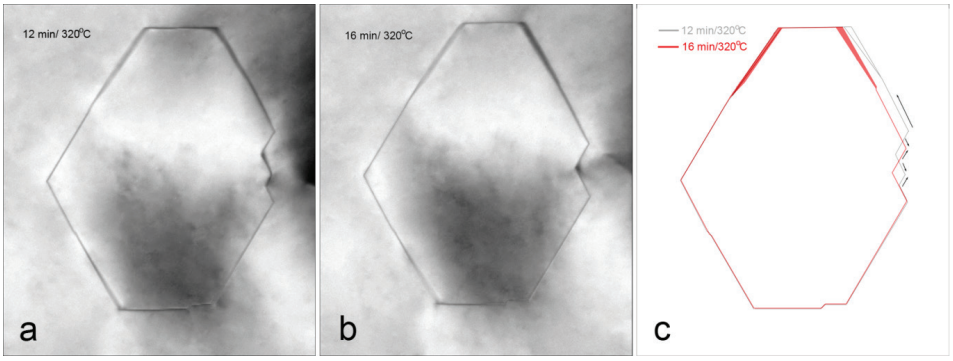

Figure 17. Illustration of grain boundary migration by lateral motion and interaction of steps.

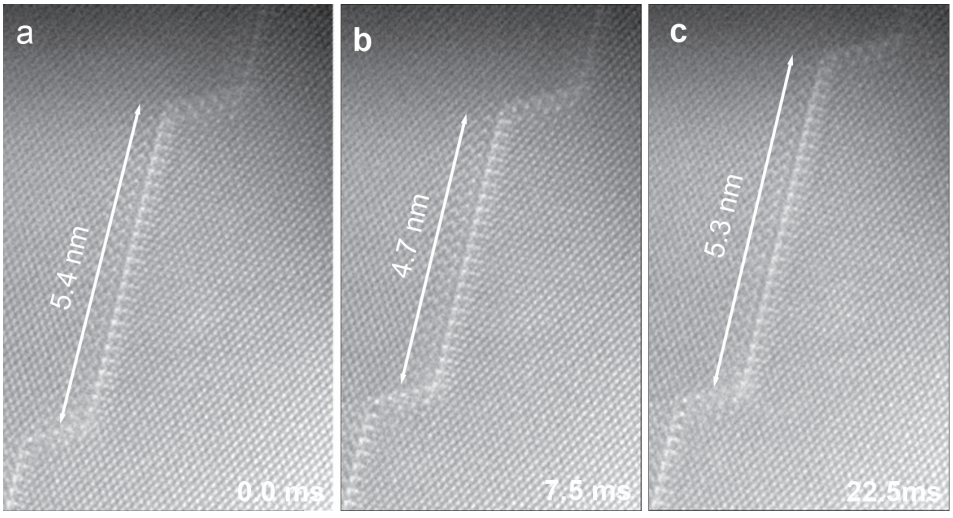

Figure 18. The sequence of images illustrating fluctuation of two steps over 10 atomic high in {111} bicrystal. Despite recording with high rate Gatan K2-IS camera (2.5ms per frame), the temporal resolution is not sufficient for these high-frequency fluctuation.

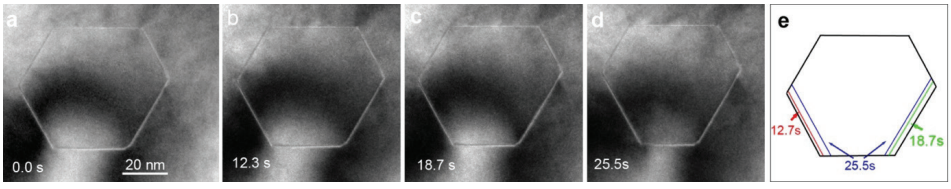

Figure 19. Grains in polygonal shape can be very stable, but once triggered facet moves as a whole. The grain collapses within a single frame after (d). The position of grain boundaries in (a-d) images is outlined in (e).

The image sequence shown in Fig. 20 can shed more light on the possible mechanism of a whole facet motion that implicates a role of buried steps. The images are formed with terminal reflections, and one of the advantages of this imaging condition is that contrast intensity depends whether the thickness is multiple of 3 atomic layers corresponding to {111} planes stacking sequence or not [73, 74]. Hence, changes in contrast observed within the grains can be related to the different thickness of the grains, revealing "double positioning" [30]. Fig. 20a shows two parallel "double positioned" boundaries, i.e. incoherent {11$\underline{2}$} boundaries terminating at different depths in the film connected by a stretch of coherent twin boundary. Such configuration corresponds to a buried step parallel to the surface of the film. Grain boundary segment on the right migrates keeping the straight configuration while buried step contracts (Fig. 20b), until almost complete annihilation (Fig. 20c). Interestingly, small step/dislocation at the boundary is dragged along. Subsequently, the "double positioned" boundary segments split again (Fig. 20d), most likely due to the repulsion of partial dislocations at the steps junctions [31], leading to the splitting of the horizontal boundary and creation of grain boundary segments parallel to the film surface corresponding to a new step.

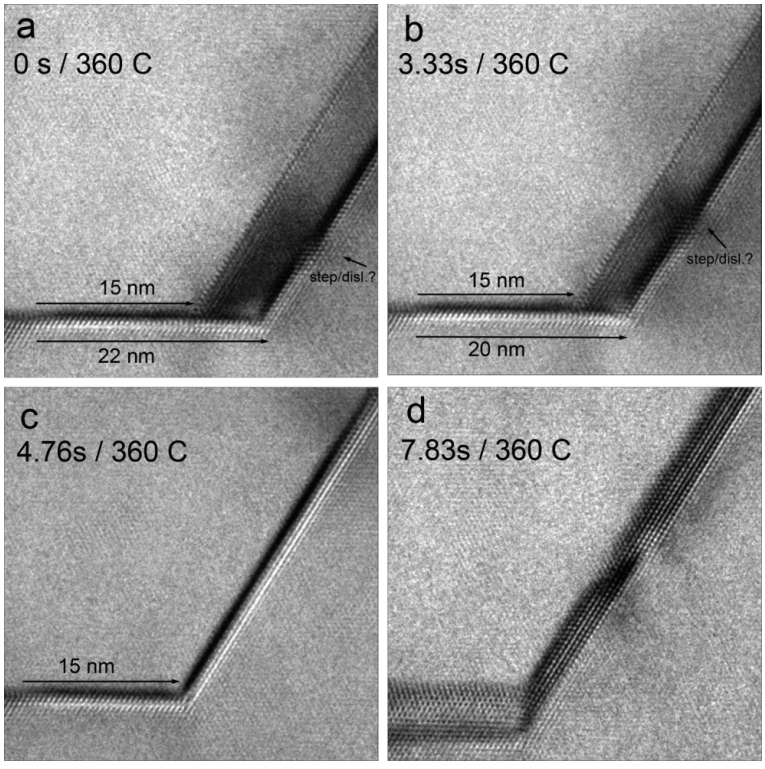

Figure 20. Migration of the grain boundary along the buried step and interaction of the "double positioned" grain boundaries.

CONCLUSIONS

The presented work documented many features of the grain boundary migration under capillary forces. Direct observations of island grain shrinkage and evaluation of mechanisms and kinetics of grain boundary motion in {110} and {111} mazed bicrystal films are reported. Characterization of grain boundary showed anisotropy increase with thermal annealing. HREM observations revealed the preference for three types facets corresponding to low-index planes in {110} bicrystals: the A- facet ($\underline{1}1\sqrt{2}$)|($1\underline{1}\sqrt{2}$), the B-facet ($1\underline{1}1$)|($1\underline{1}2$) and the C-facet ($00\underline{1}$)|($1\underline{1}0$). Migration mechanisms of the facets involve collective motion of the atoms such as regrouping by atomic shuffles, glide and step migration. High-resolution *in situ* observations revealed that the island grain shrinkage is controlled by the nucleation and propagation of steps on C-facets. While measurements showed a range of step height, there is a clear preference for steps for which the rational ratio of *n:m* approximates irrational $1:\sqrt{2}$ within 6%. The preferred step heights are closely related to the atomic structure and relaxation mechanisms of the adjacent facets. Due to the dislocation content associated with all steps, but a pure step of height 5|7, they are actually disconnections. The facet jumps of C-facet and movements of whole facets in {111} bicrystals highlighted the role of buried steps in grain boundary migration.

Measured erratic kinetic of grain shrinkage, consisting of spurs of rapid motion and stationary periods, is consistent with migration mechanisms controlled by the step nucleation. High-resolution observations of whole grains shrinking did not reveal measurable grain rotation within a last 33 ms before the total grain collapse. Shrinking grains, invariably, leave dislocation debris behind.

Acknowledgments. This work, at the Molecular Foundry – NCEM, was supported by the Office of Science of the U. S. DOE under Contract No. DE-AC02-05CH11231. The author would like to express special thanks to Dr. Uli Dahmen for guidance and support over many years without whom this work would not be possible.

REFERENCES

[1] R. W. Siegel, G. J. Thomas, Grain boundaries in nanophase materials, *Ultramicroscopy.* 40 (1992) 376–384.

[2] H. Gleiter, Nanostructured materials: basic concepts and microstructure, *Acta Mater.* 48 (2000) 1–29.

[3] Carl Koch, Ilya Ovid'ko, Sudipta Seal, Stan Veprek, Structural Nanocrystalline Materials: Fundamentals and Applications**,** Cambridge University Press, Cambridge, 2007.

[4] M. Da, L. Lu, R. J. Asaro, J. T. M. De Hosson, E. Ma, Toward a quantitative understanding of mechanical behavior of nanocrystalline metals, *Acta Mater.* 55 (2007) 4041–4065.

[5] A. P. Sutton, R. W. Balluffi, Interfaces in Crystalline Materials, Oxford University Press, Oxford, 1995.
[6] V. Yu Novikov, Grain growth in nanocrystalline materials, *Mater. Lett.* 159 (2015) 510–513.
[7] R. A. Andrievski, Review of thermal stability of nanomaterials, *J. Mater. Sci.* 49 (2014) 14449–1460.
[8] K. L. Merkle, L. J. Thompson, F. Phillipp, In-situ HREM studies of grain boundary migration, *Interface Sci.* 12 (2004) 277–292.
[9] K. L. Merkle, L. J. Thompson, Atomic-scale observation of grain boundary motion, *Mater. Lett.* 48 (2001) 188–193.
[10] K. L. Merkle, L. J. Thompson, F. Phillipp, Thermally activated step motion observed by high-resolution electron microscopy at a (113) symmetric tilt grain-boundary in aluminium, *Phil. Mag. Lett.* 82 (2002) 589–597.
[11] K. L. Merkle, L. J. Thompson, F. Phillipp, Collective Effects in Grain Boundary Migration, *Physical Review Letters.* 88 (2002) 391.
[12] J. P. Hirth, R. C. Pond, R. G. Hoagland, X. Y. Liu, J. Wang, Interface defects, reference spaces and the Frank-Bilby equation, *Prog. Mater. Sci.* 58 (2013) 749–823.
[13] K. H. Westmacott, S. Hinderberger, U. Dahmen, Physical vapour deposition growth and transmission electron microscopy characterization of epitaxial thin metal films on single-crystal Si and Ge substrates, *Phil. Mag. A.* 81 (2001) 1547–1578.
[14] T. Watanabe, Grain boundary engineering: historical perspective and future prospects, *J. Mater. Sci.* 46 (2011) 4095–4115.
[15] A. Khalajhedayati, Z. Pan, T.J. Rupert, Manipulating the interfacial structure of nanomaterials to achieve a unique combination of strength and ductility, *Nat. Comm.* 7 (2016), 10802.
[16] Gunter Gottstein, Lasar S. Shvindlerman, Grain boundary migration in Metals: Thermodynamics, kinetics and application, 2nd Ed. Boca Raton: CRC Press, 2009.
[17] G. Gottstein, D. Molodov, L. S. Shvindlerman, Grain boundary migration in metals: recent developments, *Interface Sci.* 6 (1998) 7–22.
[18] M. Upmanyu, D. J. Srolovitz, L. S. Shvindlerman, G. Gottstein, Misorientation dependence of intrinsic grain boundary mobility: simulation and experiment, *Acta Mater.* 47 (1999) 3901–3914.
[19] M. Furtkamp, G. Gottstein, D. A. Molodov, S. V. N, L. S. Shvindlerman, Grain boundary migration in Fe-3.5% Si bicrystals with [001] tilt boundaries, *Acta Mater.* 46 (1998) 4103–4110.
[20] K. Barmak, J. Kim, C. S. Kim, W. E. Archibald, G. S. Rohrer, A. D. Rollett, D. Kinderlehrer, S. Ta'asan, H. Zang, D. J. Srolovitz, Grain boundary energy and grain growth in Al films: Comparison of experiments and simulations, *Scripta Materialia.* 54 (2006) 1059–1063.
[21] M. L. Taheri, D. Molodov, G. Gottstein, A. D. Rollett, Grain boundary mobility under a stored-energy driving force: a comparison to curvature-driven boundary migration, *Z. Metallkd.* 96 (2005) 1167–1170.
[22] D. L. Olmsted, E. A. Holm, S. M. Foiles, G Survey of computed grain boundary properties in face-centered cubic metals—II: Grain boundary mobility, *Acta Mater.* 57 (2009) 3704–3713.
[23] K. L. Merkle, L. J. Thompson, High-resolution electron microscopy of twist and general grain boundaries, *Phys.Rev. Lett.* 83 (1999) 556–559.

[24] U. Dahmen, K. H. Westmacott, TEM characterization of grain boundaries in mazed bicrystal films of aluminum, *Mat. Res. Soc. Symp. Proc.* 229 (1991) 167–178.
[25] U. Czubayko, V. G. Sursaeva, L. S. Shvindlerman, Influence of triple junctions on grain boundary motion, *Acta Mater.* 46 (1998) 5863–5971.
[26] S. V. Bobylev, I. A. Ovid'ko, Mobility of Triple Junctions of Grain Boundaries during their Migration in Deformed Nanocrystalline Materials, *Rev. Adv. Mater. Sci.* 22 (2009) 39–51.
[27] C. C. Yang, A. D. Rollett, W. W. Mullins, Measuring relative grain boundary energies and mobilities in an aluminum foil from triple junction geometry, *Scripta Mater.* 44 (2001) 2735–2740.
[28] T. Radetic, U. Dahmen, Microstructure and Coarsening in Mazed Bicrystal Films of Au Grown on Ge Substrates, *Mat. Res. Soc. Symp. Proc.* 648 (2001) P11.41.1.
[29] T. Radetic, A. M. Minor, U. Dahmen, Capillarity-driven migration of a thin Ge wedge in contact with a bicrystalline Au film, *Acta Mater.* 59 (2011) 2481–2490.
[30] C. J. D. Hetherington, U. Dahmen, J. M. Penisson, Atomic structure of interfaces in mazed Au bicrystals, *Mat. Res. Soc. Symp. Proc.* 466 (1997).
[31] G. Lucadamo, D. L. Medlin, Dislocation emission at junctions between Sigma =3 grain boundaries in gold thin films, *Acta Mater.* 50 (2002) 3045–3055.
[32] W. W. Mullins, The effect of thermal grooving on grain boundary motion, *Acta Metall.* 6 (1958) 414–427.
[33] T. Radetic, C. Ophus, D. L. Olmsted, M. Asta, U. Dahmen, Mechanism and dynamics of shrinking island grains in mazed bicrystal thin films of Au, *Acta Mater.* 60 (2012) 7051–7063.
[34] F. Mompiou, M. Legros, T. Radetic, U. Dahmen, D. S. Gianola, K. J. Hemker, In situ TEM observation of grain annihilation in tricrystalline aluminum films, *Acta Mater.* 60 (2012) 2209–2218.
[35] J. W. Cahn, J. E. Taylor, A unified approach to motion of grain boundaries, relative tangential translation along grain boundaries, and grain rotation, *Acta Mater.* 52 (2004) 4887–4898.
[36] Z. T. Trautt, Y. Mishin, Capillary-driven grain boundary motion and grain rotation in a tricrystal: A molecular dynamics study, *Acta Mater.* 65 (2014) 19–31.
[37] M. Upmanyu, D. J. Srolovitz, A. E. Lobkovsky, J. A. Warren, W. C. Carter, Simultaneous grain boundary migration and grain rotation, *Acta Mater.* 54 (2006) 1707–1719.
[38] J. W. Cahn, Y. Mishin, A. Suzuki, Coupling grain boundary motion to shear deformation, *Acta Mater.* 54 (2006) 4953–4975.
[39] Y. Mishin, M. Asta, J. Li, Atomistic modeling of interfaces and their impact on microstructure and properties, *Acta Mater.* 58 (2010) 1117–1151.
[40] K. A. Wu, P. W. Voorhees, Phase field crystal simulations of nanocrystalline grain growth in two dimensions, *Acta Mater.* 60 (2012) 407–419.
[41] T. Gorkaya, K. D. Molodov, D. A. Molodov, G. Gottstein, Concurrent grain boundary motion and grain rotation under an applied stress, *Acta Mater.* 59 (2011) 5674–5680.
[42] L. A. Barrales-Mora, J. E. Brandenburg, D. A. Molodov, Impact of grain boundary character on grain rotation, *Acta Mater.* 80 (2014) 141–148.

[43] S. E. Babcock, R. W. Balluffi, Grain boundary kinetics-I. In situ observations of coupled grain boundary dislocation motion, crystal translation and boundary displacement, *Acta Metall.* 37 (1989) 2357–2365.
[44] K. E. Harris, V. V. Singh, A. H. King, Grain rotation in thin films of gold, *Acta Mater.* 46 (1998) 2623–2633.
[45] P. Liu, S. C. Mao, L. H. Wang, X. D. Han, Z. Zhang, Direct dynamic atomic mechanisms of strain-induced grain rotation in nanocrystalline, textured, columnar-structured thin gold films, *Scripta Mater.* 64 (2011) 343–346.
[46] S. E. Babcock, R. W. Balluffi, Grain boundary kinetic - II. In situ observations of the role of grain boundary dislocations in high-angle boundary migration, *Acta Metall.* 37 (1989) 2367–2376.
[47] B. B. Rath, M. Winning, J. C. M. Li, Coupling between grain growth and grain rotation, *Appl. Phys. Lett.* 90 (2007).
[48] J. P. Hirth, R. W. Balluffi, On grain boundary dislocations and ledges, *Acta Metall.* 21 (1973) 929–942.
[49] J. P. Hirth, R. C. Pond, Steps, dislocations and disconnections as interface defects relating to structure and phase transformations, *Acta Mater.* 44 (1996) 4749–4763.
[50] J. C. Russ, Stereological Interpretation of Measurement Data, in: *Computer-Assisted Microscopy* (1990) pp. 221–266, Springer US, Boston, MA, USA.
[51] G. S. Rohrer, Grain boundary energy anisotropy: a review, *J. Mater. Sci.* 46 (2011) 5881–5895.
[52] S. Ramanathan, B. M. Clemens, P. C. McIntyre, U. Dahmen, Microstructural study of epitaxial platinum and permalloy/platinum films grown on (0001) sapphire, *Phil. Mag. A.* 81 (2001) 2073–2094.
[53] T. Radetic, U. Dahmen, Unpublished work.
[54] U. Dahmen, C. J. D. Hetheringtont, M. A. O'Keefe, K. H. Westmacottt, M. J. Mills, M. S. Daw, et al. Atomic structure of a Σ99 grain boundary in aluminium: A comparison between atomic-resolution observation and pair-potential and embedded-atom simulations, *Phil. Mag. Lett.* 62 (1990) 327–335.
[55] D. L. Medlin, D. Cohen, R. C. Pond, Accommodation of coherency strain by interfacial disconnections at a 90° <110> grain boundary in gold, *Phil. Mag. Lett.* 83 (2003) 223–232.
[56] J. A. Brown, Y. Mishin, Dissociation and faceting of asymmetrical tilt grain boundaries: Molecular dynamics simulations of copper, *Phys. Rev. B.* 76 (2007) 134118.
[57] J. D. Rittner, D. N. Seidman, K. L. Merkle, Grain-boundary dissociation by the emission of stacking faults, *Phys. Rev. B.* 53 (1996) R4241–R4244.
[58] K. L. Merkle, Atomic-Scale GrainBoundary Relaxation Modes in Metals and Ceramics, *Microscopy and Microanalysis.* 3 (1997) 339–351.
[59] D. L. Medlin, S. M. Foiles, D. Cohen, A Dislocation-based description of grain boundary dissociation: application to 90 <110> tilt boundary in gold, *Acta Materialia.* 49 (2001) 3689–3697.
[60] D. L. Medlin, J. C. Hamilton, Formation of hexagonal close packing at a grain boundary in gold by the dissociation of a dense array of crystal lattice dislocations, *J Mater Sci.* 44 (2009) 3608–3617.
[61] J. M. Pénisson, F. Lançon, U. Dahmen, High resolution study of a quasiperiodic grain boundary in gold, *Mater. Sci. Forum.* 294-296 (1999) 27–34.

[62] F. Lançon, J. M. Pénisson, U. Dahmen, Quasicrystalline gold interface with a hypo-friction property, *Europhys. Lett.* 49 (2004) 603–609.
[63] A. Gautam, C. Ophus, F. Lançon, V. Radmilovic, U. Dahmen, Atomic structure characterization of an incommensurate grain boundary, *Acta Mater.* 61 (2013) 5078–5086.
[64] T. Radetic, F. Lançon, U. Dahmen, Chevron defect at the intersection of grain boundaries with free surfaces in Au, *Phys. Rev. Lett.* 89 (2002) 085502.
[65] F. Lançon, J. Ye, D. Caliste, T. Radetic, A.M. Minor, U. Dahmen, Superglide at an internal incommensurate boundary, *Nano Lett.* 10 (2010) 695–700.
[66] U. Dahmen, R. Erni, V. Radmilovic, C. Ksielowski, M. Dacil-Rossell, P. Denes, Background, status and future of the transmission electron aberration-corrected microscope project, *Phil. Trans. R. Soc.* A367 (2009) 3795–3808.
[67] J. E. Taylor, J. W. Cahn, C. A. Handwerker, Overview No. 98 I–Geometric models of crystal growth**,** *Acta Metall. Mater.* 40 (1992) 1443–1474.
[68] T. Radetic, A. Gautam, C. Ophus, C. Czarnik, U. Dahmen, High resolution observations of interface dynamics using a direct electron detection camera, *Microsc. Microanal.* 20 (2014) 1594–1595.
[69] Pan M. Czarnik C. Image Detectors for Environmental Transmission Electron Microscopy (ETEM). In: Hansen T. Wagner J. (eds): *Controlled Atmosphere Transmission Electron Microscopy*, (2016), pp. 143–164, Springer, Cham.
[70] H. Gleiter, The Mechanism of Grain Boundary Migration, *Acta Metall.* 17 (1969) 565–573.
[71] M. L. Bowers, C. Ophus, A. Gautam, F. Lançon, U. Dahmen, Step Coalescence by Collective Motion at an Incommensurate Grain Boundary, *Phys. Rev. Lett.* 116 (2016) 106102.
[72] R. C. Pond, D. L. Medlin, A. Serra, A study of the accommodation of coherency strain by interfacial defects at a grain boundary in gold, *Phil. Mag.* 86 (2006) 4667–4684.
[73] H. R. Kolar, J. C. H. Spence, H. Alexander, Observation of moving dislocation kinks and unpinning, *Phys. Rev. Lett.* 77 (1996) 4031–4034.
[74] J. C. H. Spence, Imaging moving dislocation kinks and buried interfaces by HREM, *Ultramicroscopy.* 67 (1997) 171–180.
[75] D. L. Medlin, G. Lucadamo, Morphological Evolution of a Fully Faceted Grain Boundary, *Mat. Res. Soc. Symp.* Vol. 652 (2001) Y3.4.1.
[76] C. P. Race, R. Hadian, J. von Pezold, B. Grabowski, J. Neugebauer, Mechanisms and kinetics of the migration of grain boundaries containing extended defects, *Phys. Rev. B.* 92 (2015) 174115.
[77] R. Hadian, B. Grabowski, C. P. Race, J. Neugebauer, Atomistic migration mechanisms of atomically flat, stepped, and kinked grain boundaries, *Phys. Rev. B.* 94 (2016) 165413.

Тамара Радетић

АТОМИСТИЧКИ И КРИСТАЛОГРАФСКИ ФЕНОМЕНИ ПРИ КОНТРАКЦИЈИ НАНОЗРНА

Р е з и м е

Међуповршине, односно границе зрна, имају кључну улогу у дефинисању јединствених својстава металних материјала са нанокристалном као и микроструктуром ултрафиних зрна. Услед ефекта мале величине, атомска структура и покретљивост граница зрна одређују стабилност нанокристалне микроструктуре. У овом прилогу је дат приказ феномена који се односе на механизам и кинетику миграције граница зрна у танким филмовима злата под утицајем капиларних сила. Контракција циркуларних нанозрна у танким филмовима тзв. мазед бикристалне морфологије – поликристалне структуре у којој су присутне само две оријентације зрна – на повишеним температурама карактеризована је *in situ* електронском микроскопијом, конвенционалном и високе резолуције. Карактеризација је указала да је висок степен анизотропије својствен нанозрнима, односно изражена склоност ка образовању пљосни (фацета) на одређеним типовима кристалографских равни са ниским Милеровим индексима. Утврђено је да механизам миграције пљосни укључује колективно кретање атома, односно, регруписање атома са померајима мањим од параметра кристалне решетке, клизање и миграцију степеница. *In situ* микроскопија високе резолуције је показала да је миграција контролисана нуклеацијом и пропагацијом степеница и дисконекција, тј. дефеката који поред компоненте степенице имају и дислокациону компоненту, како латерално тако и у правцу перпендикуларном на површину филма. Непостојна кинетика контакције је у сагласности са механизмом миграције контролисаним нуклеацијом степеница. Детаљна анализа дефеката на међуповршинама показала је присуство степеница различитих висина и дислокационог садржаја. Висина степенице/дисконекције ограничава њену мобилност у {110} филмовима, док такав утицај није запажен у {111} филмовима. У току контракције није примећена ротација зрна.